# Fracture Mechanisms and Structural Integrity Assessment of Equipments for NPP with Different Types of Reactors

George Karzov[1a] and Boris Margolin[1b]

[1]Central Research Institute of Structural Materials "Prometey", Saint-Petersburg, Russia

[a]kar@prometey2.spb.su, [b]margolin@prometey2.spb.su

**Keywords**: fracture, material degradation, fracture criteria, structural integrity, nuclear power plants, neutron irradiation

**Abstract**

The present report represents the micro mechanisms and local criteria of brittle, ductile, thermal fatigue and creep failure under neutron irradiation and the developed models for prediction of fracture parameters on a macro-scale. Application of the proposed criteria and models are shown for calculation of strength, structural integrity and lifetime of NPP equipments.

## Introduction

Assessment of structural integrity of equipments for nuclear power plants (NPP) with different types of reactors has a series of specific features. In particular, unlike most structures, for which material properties vary weakly during service time, structural materials of nuclear reactors degrade significantly due to long-term neutron irradiation and high temperatures. Critical events that determine structural integrity and lifetime of reactor components are controlled by various possible mechanisms of fracture and ageing of materials.

That's why to assess structural integrity of NPP components, we should be able to predict the variation of material properties for long-term service. It is clear that such information cannot be obtained from direct tests in conditions close to operation ones. Moreover the problem of transferability of test results from small-scale specimens to large-scale NPP component arises.

Therefore assessment of structural integrity of nuclear reactor components cannot be based only on traditional fracture mechanics approaches that use the test results obtained for conditions close to operation ones. It is necessary to develop the critical event criteria and physical-and-mechanical models that provide the prediction of material fracture on various mechanisms allowing for scale and time factors.

The present paper considers main approaches developed during last years that allow one to provide models and procedures for long-term prediction of basic properties of irradiated materials that are required for assessment of structural integrity and serviceability of NPP equipments.

## NPP with Pressure Water Reactor - WWER Type

**Reactor Pressure Vessels (RPV).** RPV is the main noninterchangeable component of NPP equipments. Structural integrity of RPV is assessed by the condition of inadmissibility of its brittle fracture during all period of NPP operation, the base characteristic for such assessment being fracture toughness of a material.

For RPV of WWER type the critical event is controlled by critical embrittlement of a material caused by neutron irradiation that results in start and unstable propagation of a crack in inhomogeneous stress and temperature fields that arise under pressured thermo-shock condition for emergency core cooling.

For assessment of structural integrity of reactor pressure vessels (RPV) it is necessary to predict the resistance of RPV to brittle fracture on the basis of test results of small-size surveillance specimens (the account taken of scale factor).

The simplified scheme for assessment of RPV service life is represented in Figs. 1 and 2. Scheme of RPV loading in terms of temperature and stress distributions on RPV wall is shown in Fig. 1 for the most dangerous condition of RPV loading under pressurized thermo-shock (PTS) regime that occurs for emergency RPV core cooling. In this condition cold water is poured into RPV worked at temperature $T \approx 300^{o}C$. The typical for emergency cooling dependence of stress intensity factor on temperature, $K_J(T)$, is shown in Fig. 2. In this figure the temperature dependences of fracture toughness, $K_{JC}(T)$, are shown for RPV material in unirradiated (initial) and irradiated conditions. As seen from Fig. 2, the $K_{JC}(T)$ curve shifts to higher temperature range with increasing the neutron fluence F. The limit neutron fluence that is in direct proportion to RPV life time is determined from brittle fracture criterion that may be written in the simplified form as

$$K_J(T) = K_{JC}(T) \quad \text{and} \quad \dot{K}_J(T) > 0, \tag{1}$$

where $K_J$ is stress intensity factor (SIF) for calculative (postulated) crack with size $a_p$ under emergency cooling.

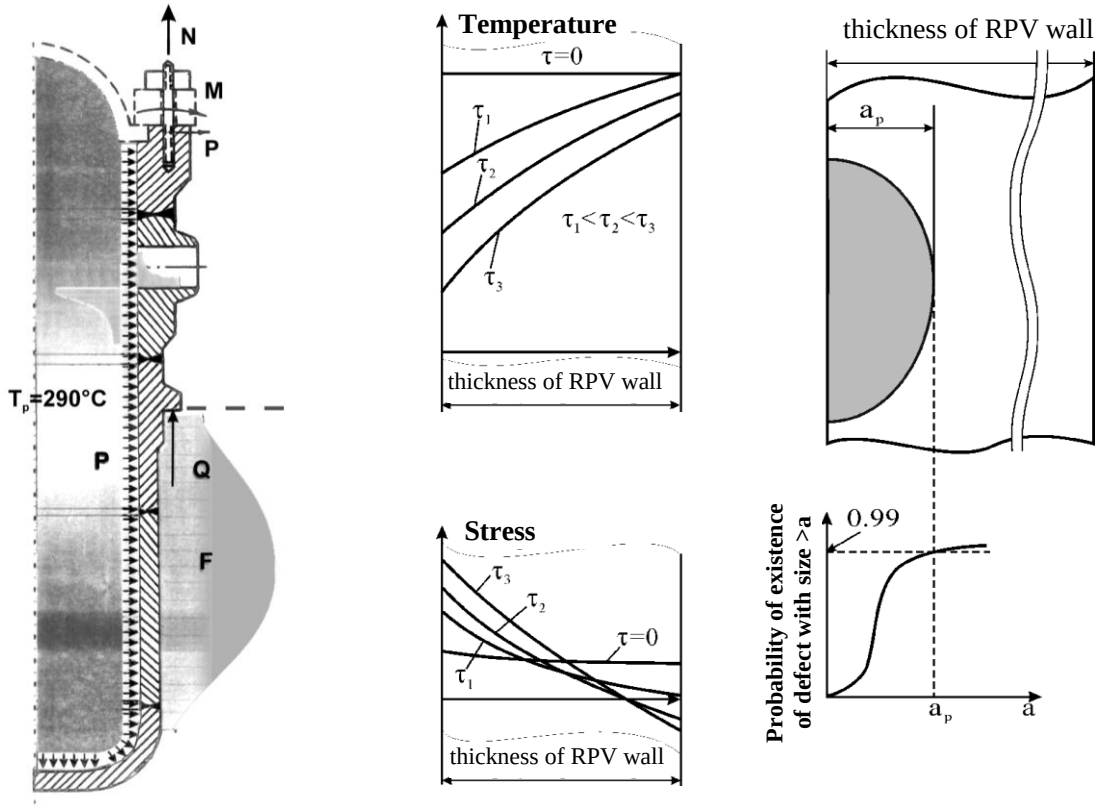


Fig. 1. Scheme of loading RPV under PTS regime.

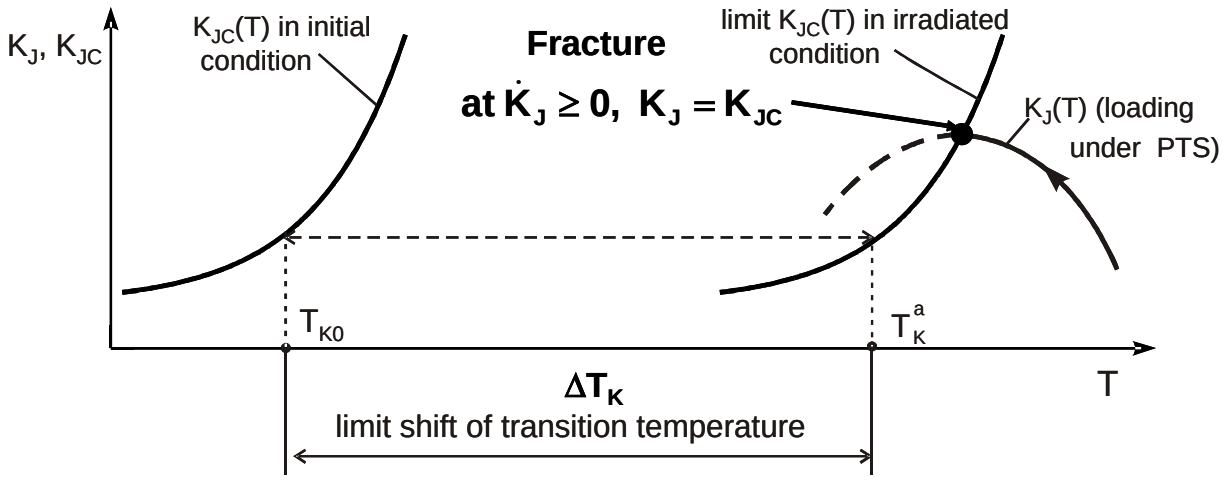


Limit fluence: $F = \left( \frac{T_k^a - T_{k0}}{A_F} \right)^n$, lifetime: $t = \frac{F}{\Phi}$, where $\Phi$ - neutron flux.

Fig. 2. Scheme for structural integrity assessment on the basis of brittle fracture criterion.

Main factor resulting in degradation of RPV materials is neutron irradiation. Neutron irradiation results in arising various radiation defects such as dislocation loops, precipitates of impurities and alloying elements (mainly, Ni, Mn, Cu and Si) and impurity segregation (mainly, P). From the mechanical viewpoint, radiation embrittlement of a material results in a shift of the $K_{JC}$(T) curve to higher temperature range.

Radiation-induced defects result in embrittlement of a material by two basic mechanisms: hardening mechanism and non-hardening mechanism. The feature of hardening mechanism is that material embrittlement is accompanied with its hardening, i.e. with yield strength growth. This mechanism is connected with radiation-induced dislocation loops and precipitates. For non-hardening mechanism, material embrittlement is not accompanied with its hardening. This mechanism is mainly connected with impurity segregation.

Material embrittlement by hardening mechanism is caused by the mechanical and physical factors. The mechanical factor consists in increasing stresses near macro-crack tip (postulated flaw in RPV) and as a result, start and propagation of cleavage microcrack (Griffith's crack) occur at lower value of $K_J$. The physical factor is arising inner self-balancing stresses that make cleavage microcrack nucleation easier.

Material embrittlement by non-hardening mechanism is caused mainly by the physical factor. Impurity segregations locate on any interfacial surfaces (for example, on carbide-matrix interfaces) and grain boundaries. Microcracks are nucleated usually on such boundaries. It is clear that the phosphorus segregation results in decreasing the interface strength and, hence, the nucleation of cleavage microcracks becomes easier compared with unirradiated steel.

The effect of radiation defects on material embrittlement is schematically shown in Fig. 3.

As seen from Figs. 1 and 2, the basic dependence of a material used in RPV integrity assessment is the $K_{JC}$(T) dependence. Until recently the resistance to brittle fracture of RPV and estimation of its lifetime are based on the following considerations.

1). $K_{JC}$ is deterministic characteristic of a material that depends on temperature only.

2). The $K_{JC}$(T) curve for irradiated material shifts to higher temperature range and a shape of the $K_{JC}$(T) curve does not change (so-called the lateral temperature shift hypothesis). By this the temperature shift $\Delta T_k$ (see Fig. 2) is equal to the shift value for the impact strength $E_a$(T) obtained from Charpy V-notched specimens.

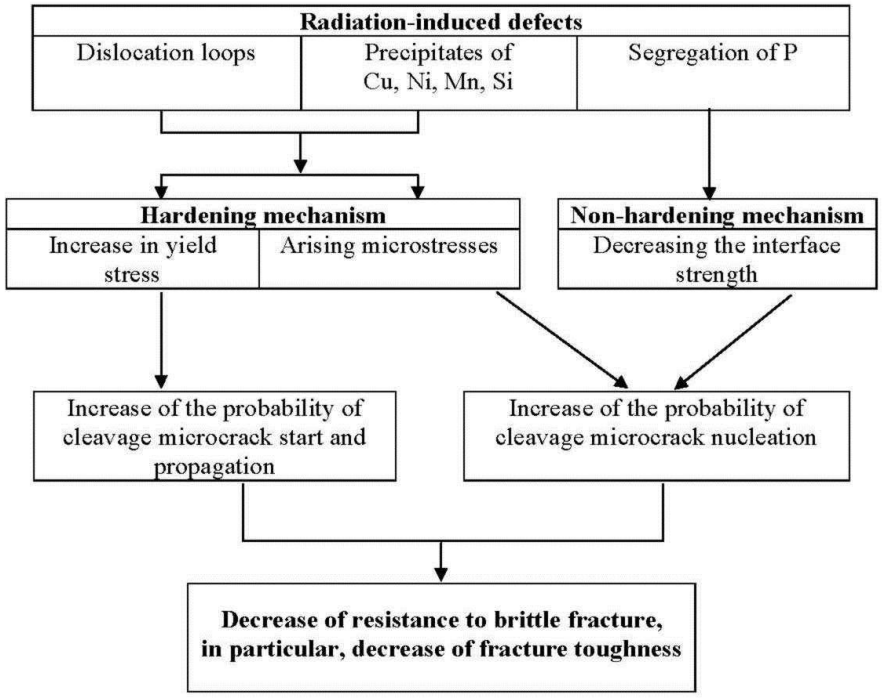


Fig. 3. The effect of radiation defects on material embrittlement (scheme).

At present, brittle fracture of RPV steel is considered as a strictly stochastic process. That's why $K_{JC}$ is stochastic properties of a material and $K_{JC}$ depends on size (strictly speaking, thickness) of tested specimens, i.e. on crack front length. Such considerations follow, for example, from wide-known Master Curve concept [1-3] and the Beremin model [4].

Moreover it was shown that fracture toughness for specimen with shallow cracks ($a$/W≤0.1÷0.2, where $a$ is a crack length, W is a specimen width) is greater than for specimens with deep cracks ($a$/W≈0.5) [5].

The $K_{JC}$(T) curve for irradiated material not only shifts to higher temperature range but also varies its shape as shown in Fig. 4 [6].

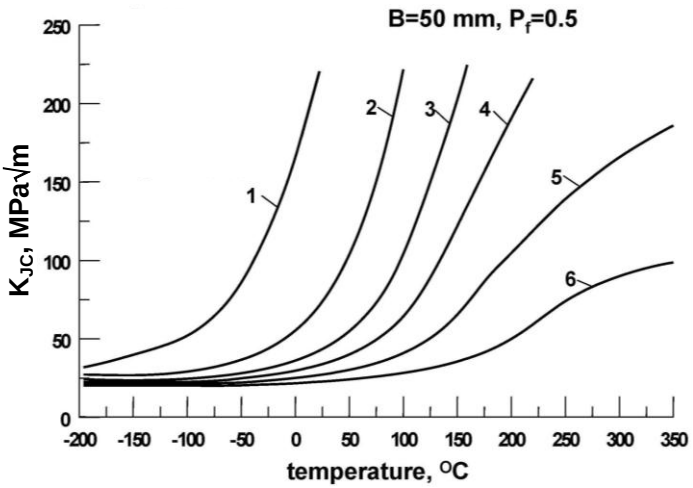


Fig. 4. $K_{JC}$(T) curves for different level of material embrittlement: 1 ÷ 6 curves correspond to increasing degree of material embrittlement.

Thus to asses adequately the structural integrity of the RPV, by criterion of resistance to brittle fracture it is necessary to take into account

a) stochastic nature of $K_{JC}$ and changing $K_{JC}(T)$ curve shape under irradiation;
b) the shallow crack effect as postulated flaws in RPV may be considered as shallow cracks;
c) the biaxial loading effect on fracture toughness as loading of a crack in RPV shell is biaxial;
d) non-homogenous SIF along the front of flaw in RPV and non-monotonic, non-isothermal loading of RPV under PTS.

Let's consider briefly the above issues.

**Prediction of $K_{JC}(T)$ for Different Degrees of Material Embrittlement.** The stochastic nature of $K_{JC}$ and the effect of a crack front length on fracture toughness was first considered in [4]. In this paper the weakest link theory proposed earlier by Weibull for homogeneous stress state [7] was used to asses the probability of brittle fracture of a cracked body when a highly heterogeneous stress field is observed. It was shown in [4] that the probabilistic distribution of fracture toughness $K_{JC}$ is described by the dependence

$$P_f = 1 - \exp\left(-\frac{B \cdot K_I^b}{C}\right), \tag{2}$$

where $P_f$ is the fracture probability of cracked specimen or $P_f$ may be considered as fracture probability of an arbitrarily chosen specimen at $K_I \le K_{JC}$; B is a specimen thickness (crack front length); C is a material constant; b is a numerical coefficient. For self-similarity of the stress-strain field near a crack tip b=4 [4].

Afterwards the approach proposed in [4] was developed by K. Wallin [1-3] as applied to prediction of the temperature dependence of fracture toughness $K_{JC}(T)$. This resulted in the development of the Master Curve method [8, 9].

In [4] local brittle fracture criterion was used in the simplest form

$$\sigma_1 = S_C, \tag{3}$$

(where $S_C$ is the critical brittle fracture stress) that did not allow one to describe adequately the transformation of $K_{JC}(T)$ curve under irradiation.

Numerous attempts undertaken by various researchers to use this criterion for prediction of the transformation of $K_{JC}(T)$ curve were not successful. To agree the predicted curve with the test results it was necessary to introduce adjusted parameters (such as the temperature dependence for the parameter $S_C$) that are not invariant relative to specimen type. For example, the parameter $S_C(T)$ differs for cracked and notched specimens. It is necessary to note that from physical point of view $S_C$ depends on T very weakly likely temperature dependence of Young modulus.

More than 20 years ago the fracture criterion controlled by stress and strain was proposed by us that allows the adequate prediction of $K_{JC}(T)$ for various degrees of material embrittlement [10]. This criterion in deterministic manner is written as [10-12]

$$\sigma_{nuc} \equiv \sigma_1 + m_{T\varepsilon}(\sigma_{eq} - \sigma_Y) \ge \sigma_d , \tag{4a}$$

$$\sigma_1 \ge S_C(æ) , \tag{4b}$$

where $m_{T\varepsilon}$ - parameter which may be interpreted as the concentrator coefficient for stress in the dislocation pile-up tip, $\sigma_Y$ - the yield stress, $\sigma_d$ - strength of carbides or another particles, on which

the cleavage microcracks are nucleated, æ=$\int d\varepsilon^p_{eq}$ - Odqvist's parameter and $d\varepsilon^p_{eq}$ - the equivalent plastic strain increment, ($\sigma_{eq}$ - $\sigma_Y$) is strain hardening of material controlled by plastic strain.

Condition (4a) in the local cleavage fracture criterion is the nucleation condition for cleavage microcracks, condition (4b) - the propagation condition for cleavage microcracks. Condition (4b) describes both the cleavage microcrack start $\sigma_1=S_0\equiv S_C$(æ=0) and their propagation through various barriers (such as grain boundaries, cell boundaries, microstresses) existing and formed in a material during plastic deformation.

Criterion (4) allows one to take into account both the mechanical and physical factors of embrittlement. The mechanical factor is taken into account by the parameter $\sigma_1$ included in criterion. The physical factor is taken into account by the parameters $\sigma_d$ and $S_C$ that as a common case decrease under irradiation.

To take into account a stochastic nature of brittle fracture and to predict the $K_{JC}(T)$ dependence criterion (4) was formulated in probabilistic manner [6,13-14]. By this, as well as in the Beremin model, the Weibull statistics for stochastic parameters and the weakest link theory were used. The probabilistic model based on criterion (4) was named the Prometey model.

The calculation results performed with the Prometey model allow one to propose new engineering method named the Unified Curve [15]. These calculation results show that all the $K_{JC}(T)$ curves for brittle fracture (when modeling ductile fracture was excluded wittingly) may be represented by vertical evolvent as one unified curve. Fig. 5 demonstrates how it may be done.

According to the Unified Curve concept the temperature dependence of fracture toughness at $P_f$=0.5 for specimens with thickness B=25 mm from RPV steel for any degree of embrittlement is described by

$$K_{JC(med)}(T) = K_{JC}^{shelf} + \Omega \cdot \left(1 + \tanh\left(\frac{T-130}{105}\right)\right), \text{ MPa}\sqrt{\text{m}}, \qquad (5)$$

where $K_{JC}^{shelf}$ =26 MPa√m; Ω is a constant for a given condition of a material; T is temperature in $^oC$.

For the embrittled materials the only parameter, Ω, varies, the rest of the numerical parameters in eqn (5) are fixed. The parameter Ω is calibrated from fracture toughness test results. For the Unified Curve the scatter in $K_{JC}$ values and the thickness effect are the same as for the Master Curve.

The Unified Curve method as well as the Prometey model predicts a possible variation in $K_{JC}(T)$ curve shape under irradiation. Comparison of $K_{JC}(T)$ curves predicted with the Master Curve and Unified Curve with the test results for materials with various degree of embrittlement is illustrated for several data sets in Fig. 6 [15]. It is shown that the Master Curve concept is a partial case of the Unified Curve concept.

As seen from Fig. 6 for material in initial condition ($T_o$=-61.3$^oC$, Ω=1472 MPa√m) the curves predicted with the Master Curve and Unified Curve coincide and adequately describe test results. For material in embrittled condition ($T_o$=+137$^oC$, Ω=73.4 MPa√m) the Master Curve method provides non-conservative and non-adequate prediction. At the same time the Unified Curve method provides adequate prediction of $K_{JC}(T)$.

It should be emphasized that both Master Curve and Unified Curve take into account the effect of specimen thickness (crack front length) on $K_{JC}$ and therefore allows in principal the transferability of fracture toughness data from small-size specimens to RPV with postulated crack.

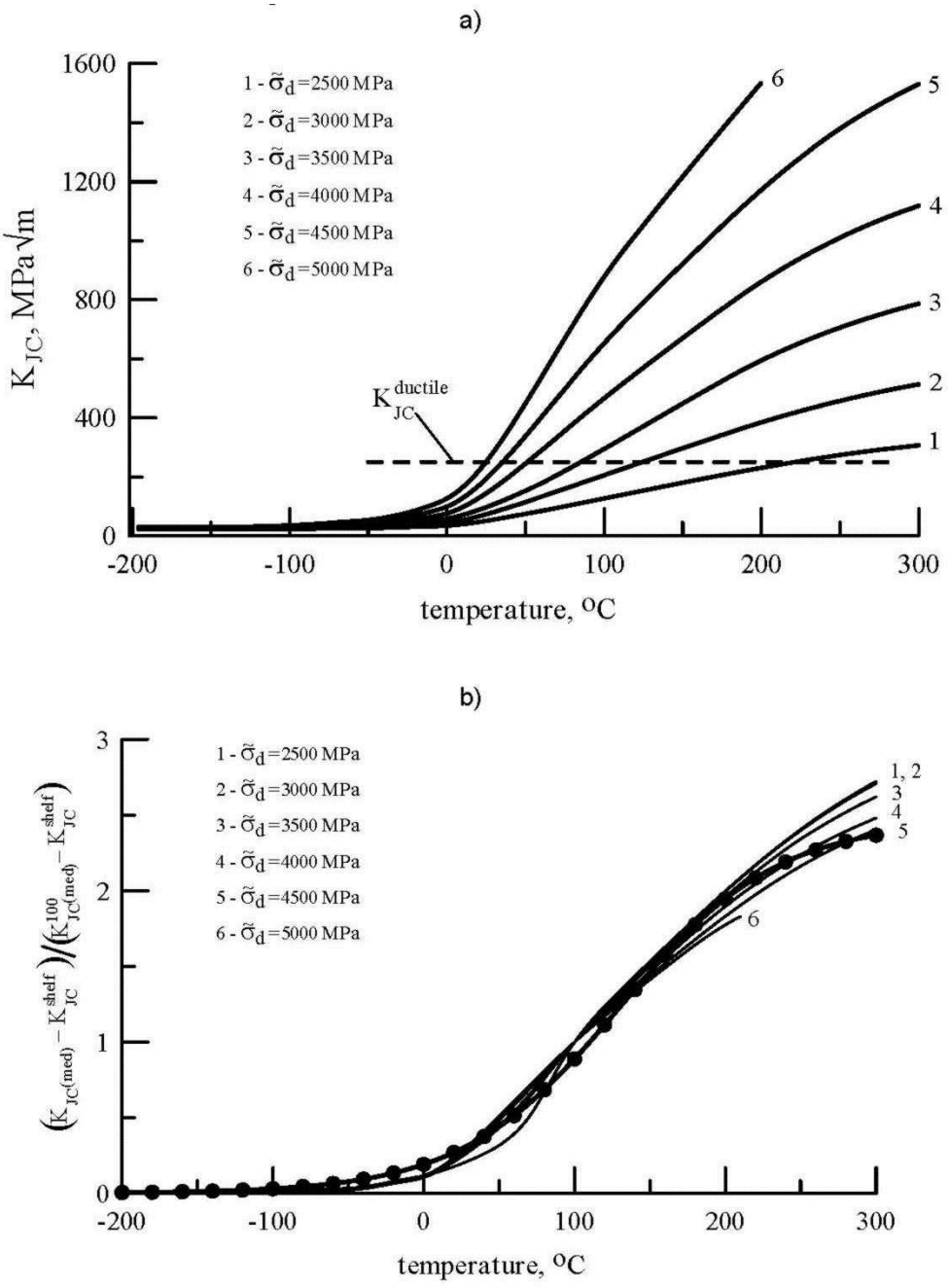


Fig. 5. The $K_{JC}(T)$ curves for radiation-embrittled RPV material calculated with the Prometey model (the dotted curve is the upper shelf level) (a) and these curves represented by the normalizing ratio $\left(K_{JC(med)} - K_{JC}^{shelf}\right)/\left(K_{JC(med)}^{100} - K_{JC}^{shelf}\right)$ and a fitting unified curve (the solid curve with points) calculated by Eq. (5) (b) [15].

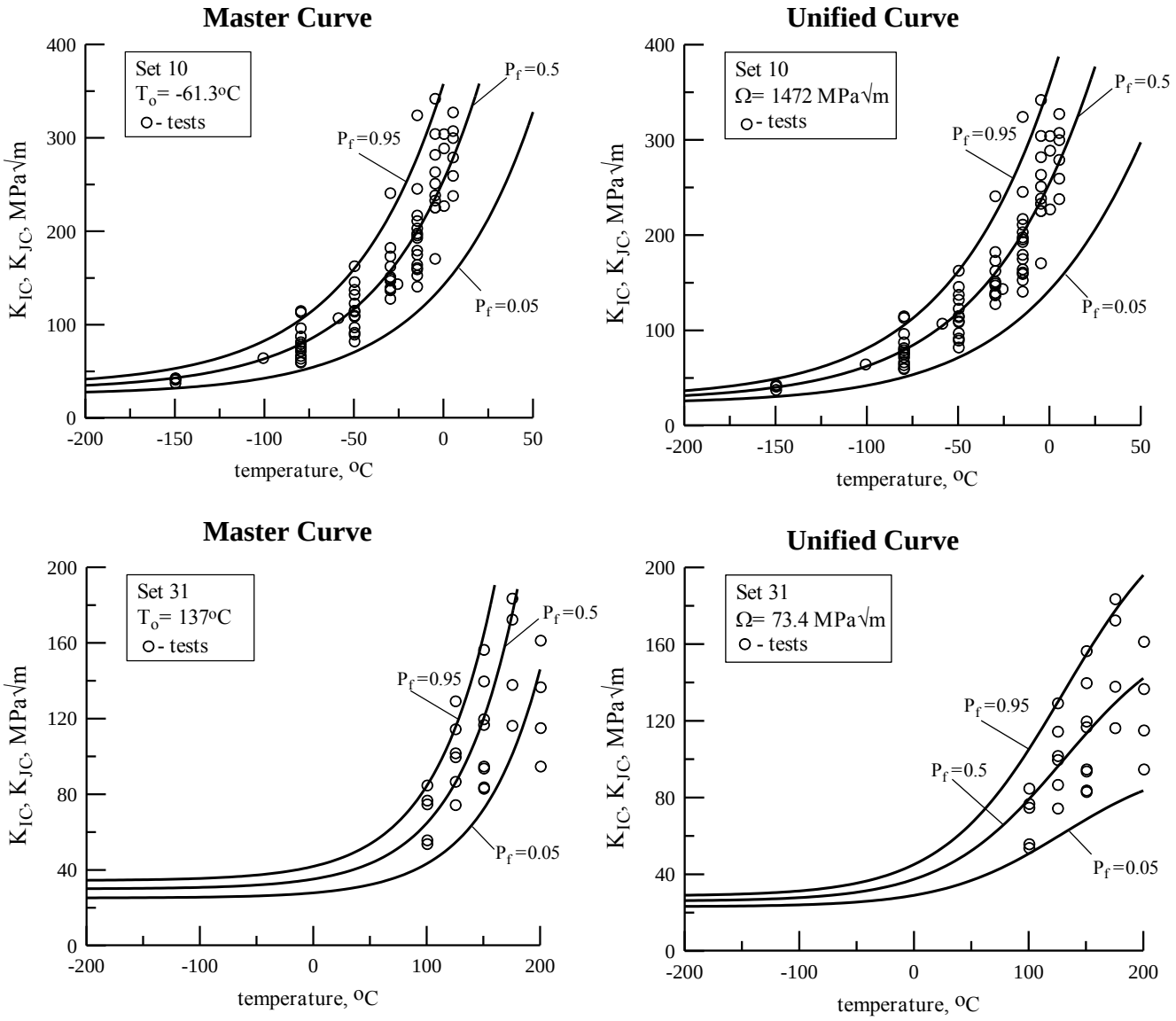


Fig. 6. Comparison of experimental data and $K_{JC}(T)$ curves for B=25 mm calculated by the Master Curve (on the left) and Unified Curve (on the right): set 10 - HSST 73W weld (initial condition), set 31 - KS01 weld (irradiated condition). The test results are recalculated for a specimen thickness B=25 mm [15].

**The Shallow Crack Effect.** The shallow crack effect is typical mechanical factor considered in [16, 17]. For specimen under plane strain condition and deep crack the stress field near crack tip represented in the form $\frac{\sigma_1}{\sigma_{eq}} = f\left(\frac{r\sigma_Y}{J}\right)$ does not depend on J-integral value. For shallow crack the above dependence depends on J-integral: when J-integral increases $\frac{\sigma_1}{\sigma_{eq}}$ decreases. For small scale yielding (SSY) the dependence $\frac{\sigma_1}{\sigma_{eq}} = f\left(\frac{r\sigma_Y}{J}\right)$ is the same for deep and shallow cracks as seen from Fig.7.

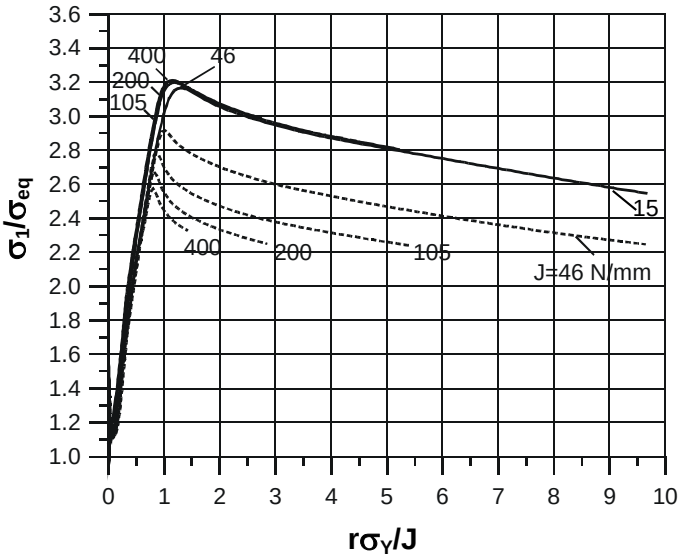


Fig. 7. The ratio $\sigma_1/\sigma_{eq}$ near deep (solid lines) and shallow (dotted lines) cracks for various values of the J-integral indicated near curves [18].

In Fig. 8 the $K_{JC}(T)$ curves are presented for deep and shallow cracks calculated by the Prometey model. Properties shown in Fig.8 correspond to experimental data shown in Fig.9.

It is seen from Figs. 7 and 8 that for low fracture values the $K_{JC}(T)$ curves coincide for deep and shallow cracks. For this case SSF near the crack tip is close to SSY. When $K_{JC}$ increases the difference between $K_{JC}$ values for deep and shallow crack increases too. It is important to note, that the scatter of $K_{JC}$ for shallow crack is larger than for deep crack.

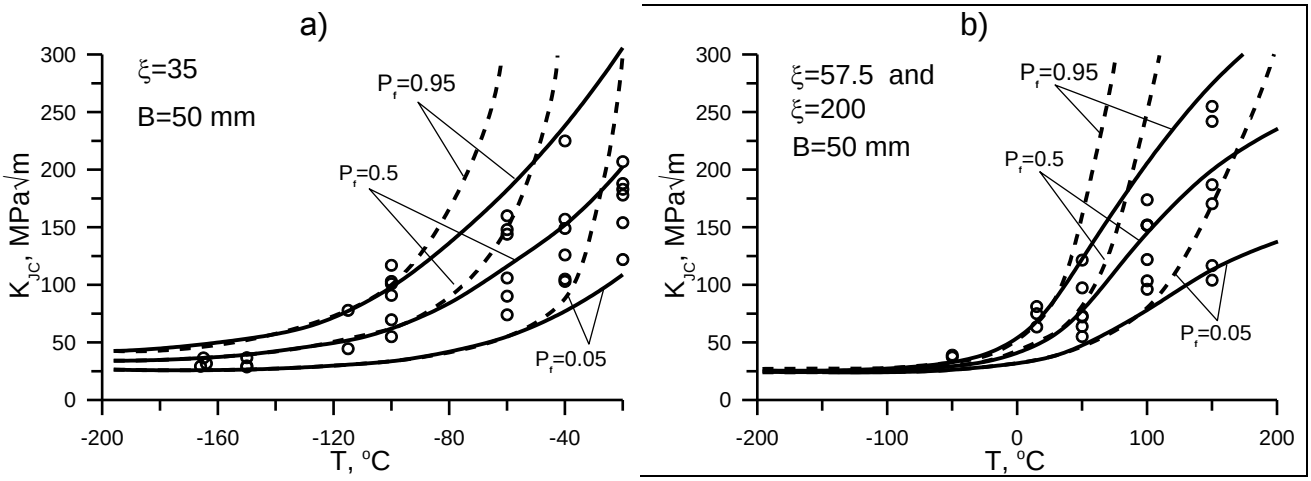


Fig. 8. The effect of shallow crack on fracture toughness: 2Cr-Ni-Mo-V steel in the initial (a) and embrittled (b) conditions: points - test results for standard 2T-CT specimens (with deep crack), the solid and dotted lines are the $K_{JC}$ (T) curves calculated by the Prometey model for deep and shallow cracks [18].

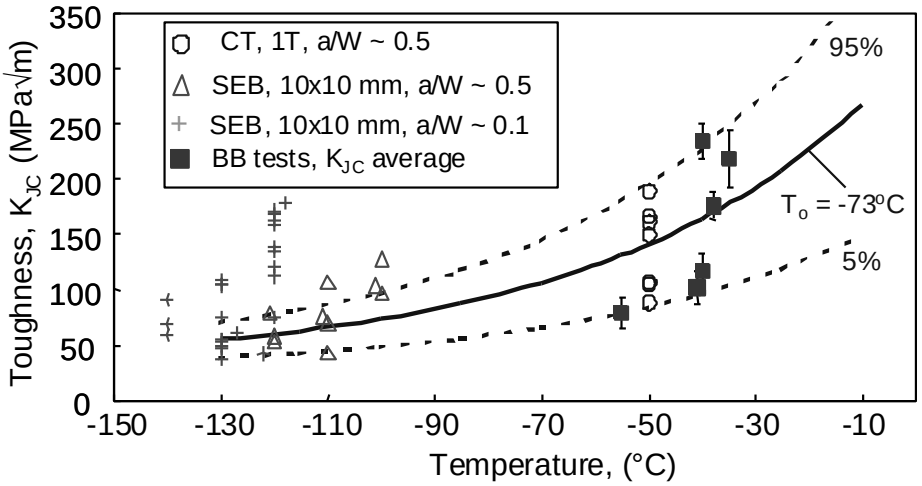


Fig. 9. Comparison of the $K_{JC}(T)$ curves calculated on the basis of the Master Curve and test results obtained of SEB specimens for deep and shallow cracks (△, +), 1T-CT specimens for deep cracks (o) and biaxial bend specimens (■) for RPV A 533 B steel [23].

Let's consider various approaches for prediction of $K_{JC}^{shallow}(T)$. According to VOCALIST Handbook [19] $K_{JC}^{shallow}(T)$ is calculated by the lateral shift of $K_{JC}^{deep}(T)$ to lower temperature range. By this it is assumed that the shapes of $K_{JC}^{shallow}(T)$ and $K_{JC}^{deep}(T)$ curves do not vary for any value of the fracture probability $P_f$. Thus, it is taken $K_{JC}^{shallow}(T) = K_{JC}^{deep}(T + \Delta T)$, where $\Delta T$ depends on specimen type.

It is clear that such assumption is in contradiction to the data in Fig. 9. Indeed, firstly, the lateral shift to lower temperature range results in difference between $K_{JC}^{shallow}$ и $K_{JC}^{deep}$ for low $K_{JC}$ values. Secondly, the scatter for $K_{JC}^{shallow}$ and $K_{JC}^{deep}$ is the same for any level of $K_{JC}$.

In papers [20-22] the alternative method for calculation of the shallow crack effect was proposed. This method is based on the assumption that fracture toughness for specimens with shallow cracks $K_{JC}^{shallow}$ may be represented in the form

$$K_{JC}^{shallow} = \omega_{sh} \cdot K_{JC}^{deep} \qquad (6)$$

where $K_{JC}^{deep}$ is fracture toughness for specimens with deep cracks.

The parameter $\omega_{sh}$ is calculated by formula

$$\omega_{sh} = [m \cdot \exp(1/m) \cdot \arccos(\exp(-1/m)) \cdot \sqrt{1 - \exp(-2/m)} - 1]^{1/2}, \qquad (7)$$

where $m = \dfrac{8a}{\pi\left(K_{JC}^{deep}/\sigma_Y\right)^2}$.

Thus, the parameter m is controlled by the relation between a crack depth *a* and the size of a plastic zone (or more specifically, the loading level of a specimen): the lower is m, the higher is $\omega_{sh}$ and hence the greater is the effect of shallow cracks.

For low temperatures when the $K_{JC}^{deep}$ value is small the parameter $\omega_{sh} \approx 1$ and there is practically

no effect of shallow cracks. $K_{JC}^{deep}$ increases with increasing temperature and, according to Eq. (7), the parameter $\omega_{sh}$ increases. As a result, with an increase in temperature the value $K_{JC}^{shallow}$ is beginning to differ more and more from $K_{JC}^{deep}$.

As $P_f$ increases (at a fixed temperature) the $K_{JC}^{deep}$ value grows and the parameter m falls. In this case the higher is $K_{JC}^{deep}$, the more marked is the growth of the value $\omega_{sh}$. As a result, the scatter of fracture toughness values for shallow cracks becomes larger than for deep ones.

Thus, the proposed engineering method takes account of the main experimental and theoretical features (obtained on the basis of the Prometey model) on the shallow crack effect on fracture toughness.

**The Effect of Stress Biaxiality on Fracture Toughness.** As is known, a RPV is subjected to biaxial loading under all calculated operating conditions. Thus, for a postulated flaw the load operates both perpendicularly to a flaw plane and parallel to a flaw plane along its front. At the same time, for standard fracture toughness tests the load operates only perpendicularly to a crack plane. Experimental investigations of the stress biaxiality effect on fracture toughness carried out on cruciform specimens [24] show that the biaxial loading results in a decrease of fracture toughness.

It was shown that a decrease of fracture toughness under the biaxial loading takes place only in specimens with shallow cracks in the case of large-scale yielding [25]. In the case of small-scale yielding or deep cracks the biaxial loading does not result in a decrease of fracture toughness.

Prediction of the stress biaxiality effect on $K_{JC}$ was performed in [25] on the basis of the Prometey local stress-and-strain controlled fracture criterion. The predicted and experimental data is compared in Fig. 10.

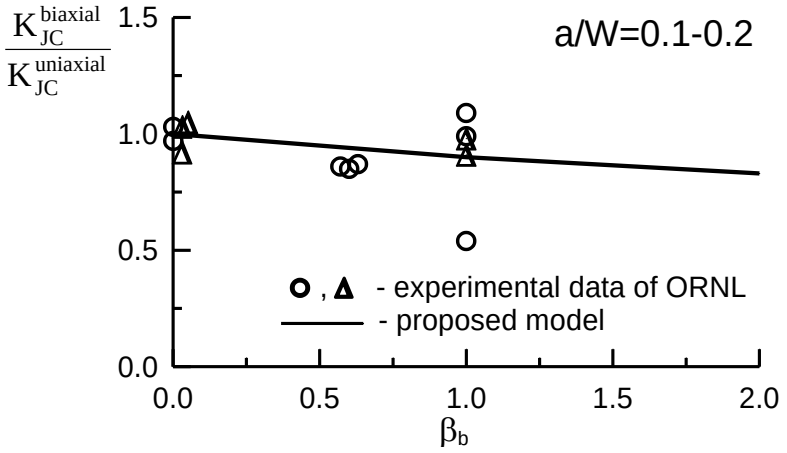


Fig. 10. The dependence of $\omega_{biax} = K_{JC}^{biaxial} / K_{JC}^{iniaxial}$ on $\beta_b$ (where $\beta_b=\sigma_L/\sigma_N$ is the biaxiality factor, $\sigma_L$ is stress along crack front, $\sigma_N$ is stress normal to crack plane): points – test results [24]; curve – prediction with the Prometey model [25].

**RPV Structural Integrity Assessment by Brittle Fracture Criterion.** Stochastic nature of brittle fracture and the $K_{JC}$ parameter should be taken into account in formulation of RPV structural integrity condition. In Russia the world's first Standard for assessment of RPV structural integrity allowing for stochastic nature of brittle fracture was created. This Standard is based on application of the Weibull dependencies (used in the Master Curve) for heterogeneous distribution of SIF along a crack front as well as non-radial loading of a material near a crack tip that occurs under emergency

cooling of a reactor (PTS condition). Later this approach was included in the IAEA Guide [26] and "Unified procedure for lifetime assessment of components and piping in WWER NPPs "VERLIFE" [27].

Criterion of RPV structural integrity is formulated as [20-22]

$$P_f < \overline{P}_f \tag{9}$$

where $P_f$ is fracture probability of RPV with given postulated flaw for considered event (for example PTS), $\overline{P}_f$ is a given level of fracture probability.

Eq. (9) with regard to equations for probability, thickness [2] and the physical features of brittle fracture after preliminary warm pre-stressing (WPS) [28] makes it possible to obtain the RPV integrity condition in the form [21, 22]

$$\frac{1}{B}\int_0^B Z(L)dL < 1 \tag{10}$$

where

$$Z(L) = \max_{(0,\tau)} \frac{(K_J(L) - K_{min})^4}{(K_{JC}^B(L) - K_{min})^4} \tag{11}$$

Here B is a length of a postulated flaw front; $K_J(L)$ is distribution of SIF along the L-coordinate (Fig. 11a) at the instant of time $\tau$; $K_{JC}^B(L)$ is distribution of the value of fracture toughness of standard specimen with thickness equal to B (for $P_f = \overline{P}_f$) along the L-coordinate at the instant of time $\tau$. Variations of fracture toughness along the L-coordinate can occur due to changes in temperature and (or) an irradiation level. For each value of a L-coordinate the value of the function Z(L) is calculated by Eq. (11) where the maximum is looked for over a period of time from 0 to the current time $\tau$. The time intervals for which

$$\begin{gathered} K_J(\tau) < 0.9 \max(K_J(0,\tau)) \\ \text{or} \\ \dot{K}_J(\tau) < 0 \end{gathered} \tag{12}$$

are excluded, since fracture after preliminary loading may occur when

$$\begin{gathered} K_J(\tau) \geq 0.9 \max(K_J(0,\tau)) \\ \text{and} \\ \dot{K}_J(\tau) > 0 \end{gathered} \tag{13}$$

(see Fig.11b).

It is necessary to note that here $\tau$ is time when PTS regime happens. Usually max $\tau$ for this case is less than one hour.

Fracture condition after WPS is validated by the study results in [28] on the basis of the experimental results obtained in [29] and represented in Fig. 12. As seen from Fig. 12 fracture at $K_f < 0.9\ K_{WPS}$ occurs only for 2% of specimens.

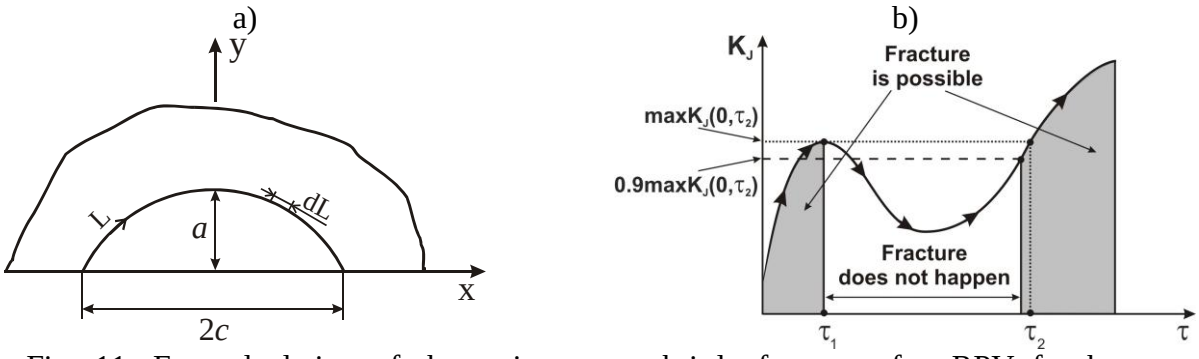


Fig. 11. For calculation of the resistance to brittle fracture of a RPV for heterogeneous distribution of SIF along the crack front (a) and possible dependence of $K_J$ on $\tau$ under non-monotonic loading (b)

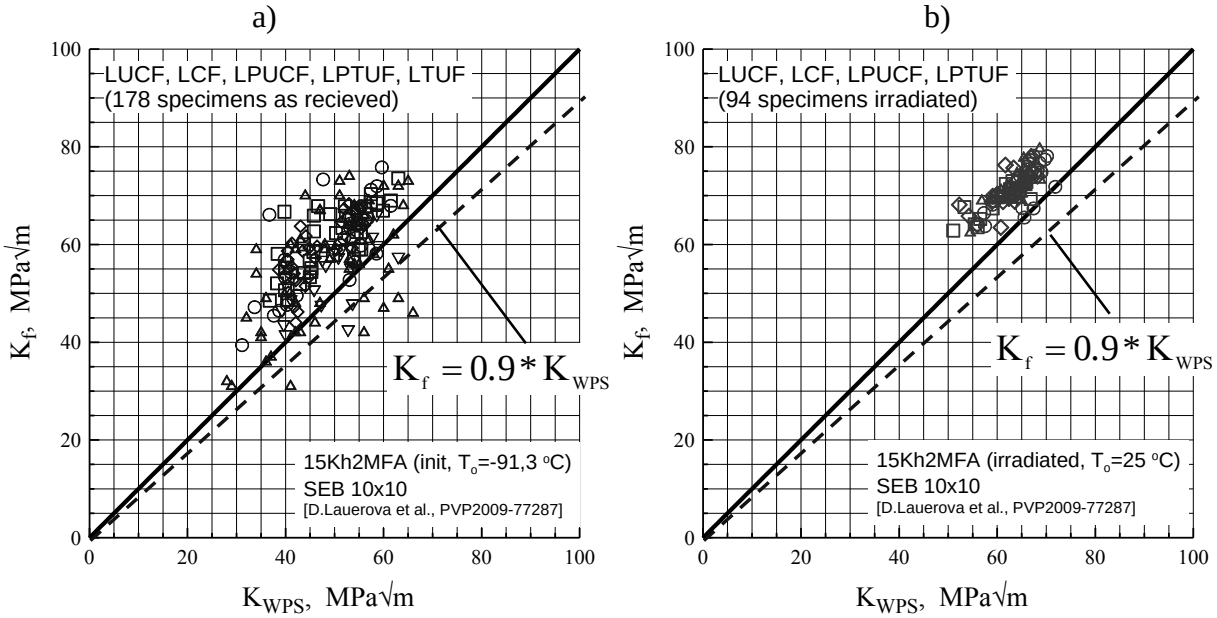


Fig. 12. The WPS effect for various WPS regimes (material in the received (a) and irradiated conditions (b)): $K_f$ – SIF at the fracture after WPS (experimental data) and $K_{WPS}$ – maximum SIF at WPS loading [29].

**Intermediate Conclusion.** The performed studies allowed one to obtain the key characteristic for assessment of RPV structural integrity, namely, the temperature dependence of fracture toughness $K_{JC}(T)$. This dependence is determined for any degree of radiation embrittlement and any given probability of brittle fracture $P=\overline{P}_f$ with the Unified Curve method on the basis of test results of small-size surveillance specimens [15]. The developed engineering approaches provide the calculation of the $K_{JC}(T)$ curve allowing for the effect of shallow crack and biaxial loading [22] as

$$K_C = \omega_{sh} \cdot \omega_{biax} \cdot K_{JC}^B \qquad (14)$$

Analysis of RPV structural integrity is performed with Eq. (10) - (12) by substituted the parameter $K_C$ instead of $K_{JC}^B$. Lifetime of RPV is maximum operation time for which structural integrity condition (10) is met.

**WWER RPV Internals**

Internals fix fuel assemblies, provide distribution of the coolant flows and also protect RPV from neutron flux, control devices and detectors. All internals components are made from austenitic steel of 18Cr-10Ni-Ti grade (chemical composition is close to 321 steel) and its weld metal. This steel in initial (unirradiated) condition has high plasticity and high resistance to corrosive cracking.

Internals of WWER are undergone high neutron irradiation. For WWER-1000 internals the maximum neutron dose for 30 years operation exceeds 60 dpa [30]. Maximum irradiation temperature considerably exceeds temperature of RPV wall and reaches 400°C. Main microstructural processes going in austenitic steels under neutron irradiation and their effect on physical-and-mechanical properties are schematically shown in Fig. 13.

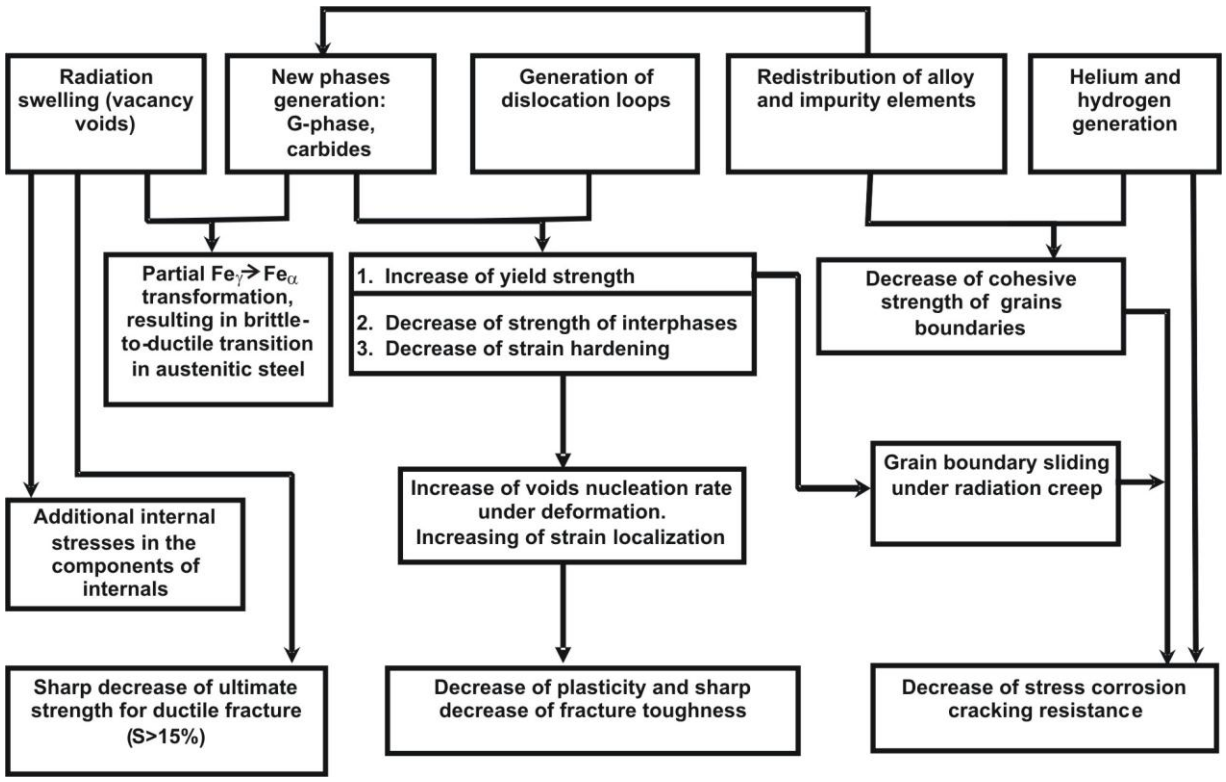


Fig. 13. Microstructural processes going in austenitic steels under neutron irradiation and their effect on physical-and-mechanical properties

Strong neutron irradiation and sufficiently high temperature result in radiation damage of internals materials. The gradient of neutron dose and temperature in internals components results in thermal stresses and swelling stresses. Mechanical loading in internals components for normal operation condition is small as it is caused mainly by weight loading. Therefore, thermal stresses and swelling stresses are main stresses acting in internals components. Strong neutron irradiation results in sharp decrease of plasticity and fracture toughness and stimulates corrosion cracking. Moreover, radiation swelling additionally decreases plasticity and fracture toughness due to the phase $Fe_\gamma \rightarrow Fe_\alpha$ transformation [31-34] and also may result in sharp decreasing of material strength and practically nil plasticity.

Thus, for adequate analysis of structural integrity and serviceability of internals the issues have to be considered and solved as follows:

– prediction of radiation swelling and creep;

– prediction of fracture toughness;

– prediction of resistance to corrosion cracking;
– material embrittlement due to radiation swelling;
– formulation of integrity criterion for internals components.
Let us consider briefly the above issues.

**Radiation Swelling and Creep.** Stress-free swelling that is swelling without any kinematic restriction. Stress-free swelling depends on neutron dose, dose rate and irradiation temperature.

Special experiments were performed during 20 years on neutron irradiation of Russian 18Cr-9Ni and 18Cr-9Ni-Ti steels (chemical compositions are close to 304 and 321 steels) with various dose rates under various irradiation temperatures. Treatment of the obtained experimental data has shown that the most appropriate dependence is written in the form [35]

$$S_0 = C_D D^n \exp\left(-r \cdot \left(T_{irr} - T_{max}\right)^2\right) \qquad (15)$$

where $S_0$ is stress-free irradiation-induced swelling, D is neutron dose, $T_{irr}$ is irradiation temperature, $C_D$, n, r and $T_{max}$ are material constants.

Values of these constants were determined as [35]:
for 18Cr-9Ni steel $C_D=8.13\cdot10^{-5}$, $r = 1.1\cdot10^{-4}$ $C^{-2}$ ;
for 18Cr-9Ni-Ti steel $C_D=1.035\cdot10^{-5}$, $r = 1.825\cdot10^{-4}$ $C^{-2}$.
Values of n and $T_{max}$ for both steels coincide and may be taken as n=1.88 and $T_{max}$=470°C.

Comparison of the experimental data and the dependencies (15) is shown in Fig. 14. The above coefficients in Eq. (15) correspond to the median value of $S_0$ (P=0.5). The values of swelling for 95% confidence interval are larger for 18Cr-9Ni steel and 18Cr-9Ni-Ti steel by 2 and 2.5 times than median values respectively.

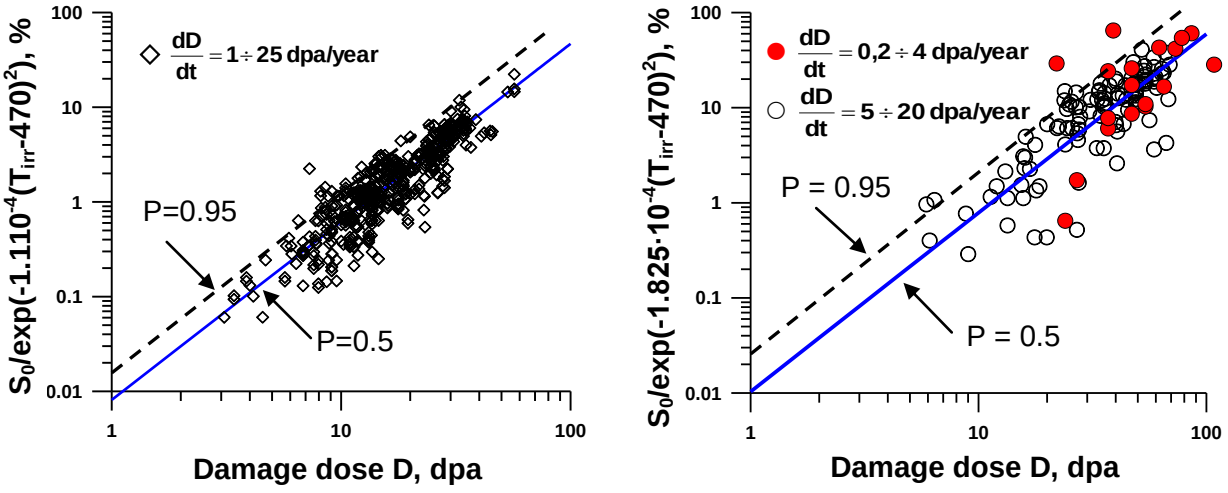


a) b)

Fig. 14. The temperature-and-dose dependence of swelling for irradiated austenitic 18Cr-9Ni steel (a) [35] and 18Cr-10Ni-Ti steel (b).

It is known that stress (acting in a component or arising due to restricted displacement of a component with swelling) varies swelling rate. The effect of stress on swelling is very important issue for adequate calculation of stress and strain fields in internals components.

At the present, there are two basic hypotheses. According to the first hypothesis the stress sign does not affect swelling. According to the second hypothesis the stress sign affects swelling.

Application of the first or second hypotheses may give very different stress fields in internals component. Let us consider, as example, core baffle of WWER-1000 which is thick shell. Due to γ-heating maximum irradiation temperature ($T_{irr}$≈400 $^0$C) is in the mid of the shell wall. When approaching to the surface of shell, $T_{irr}$ decreases up to ≈320 $^0$C. As a result, maximum swelling locates in the mid of shell wall that results in compressive stresses. Near the surface of shell tensile stresses arise. If swelling is described according to the first hypothesis, then any stress (compressive or tensile) accelerates swelling that result in an increase of stresses. So, in this case we have positive feedback. If the second hypothesis is valid, then compressive stresses reduce the swelling rate, tensile stresses increase the swelling rate. For this case stresses caused by swelling results in decrease of gradient of swelling and, hence, result in decrease of stress increment. So for this case we have negative feedback. Thus the problem arises to determine the effect of various types of stress state on swelling.

Calculative and experimental study in [36] allow one to obtain the following equation describing the stress effect on swelling

$$S = S_0(1 + P \cdot \sigma_{eff}), \tag{16}$$

where S is swelling with regard for stress effect,

$$\sigma_{eff} = (1-\eta) \cdot \sigma_m + \eta \cdot \sigma_{eq}, \tag{17}$$

$\sigma_m$ is hydrostatic stress, $\sigma_{eq}$ is equivalent stress, P and η are material constants.

Eq. (16) may be represented as

$$\frac{\Delta S_\sigma}{\Delta S_0} = P \cdot \sigma_{eff}, \tag{18}$$

where $S_\sigma$=S-$S_0$ and $S_\sigma$ is swelling caused by stress only.

Comparison of Eq. (18) and experimental data from [37] is shown in Fig. 15 for various stress states (uniaxial tension and compression, biaxial stress state, torsion). It is seen that the proposed dependence is in good agreement with experimental data. For the curve in Fig. 15 the parameter η is found as 0.15. As a common case, the parameter η depends on swelling, and this dependence may be analyzed from the physical point of view.

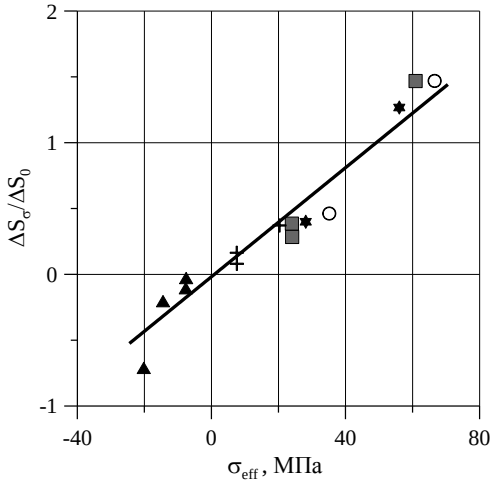


Fig. 15. The effect of different stress state on swelling [37]. Ratio of circumferential stress in a specimen to axial stress: ■ – 0/1(1/0); ○ – 2/1; ✶ – 1/1; ▲ –0/-1; ✚ – 1/-1.

In Fig. 16 the experimental data on average void diameter and void concentration are presented [36, 38]. From this figure it is seen that when $S < S^* \approx 1\%$ the void concentration increases and the average void diameter practically doesn't change. Therefore void nucleation provides the major contribution to swelling. It is clear that void nucleation is accelerated by shear stresses. In this case swelling is mainly affected by $\sigma_{eq}$ and, hence $\eta \to 1$. When $S > S^* \approx 1\%$ void concentration is steady or decreases, average void diameter increases. Steady concentration is connected with two processes: nucleation and coalescence of voids. The major contribution to swelling in this case is caused by void growth, and void nucleation gives the minor contribution. Void growth is accelerated by hydrostatic stress $\sigma_m$. In this case both $\sigma_m$ and $\sigma_{eq}$ affect swelling and $\eta = 0.15$.

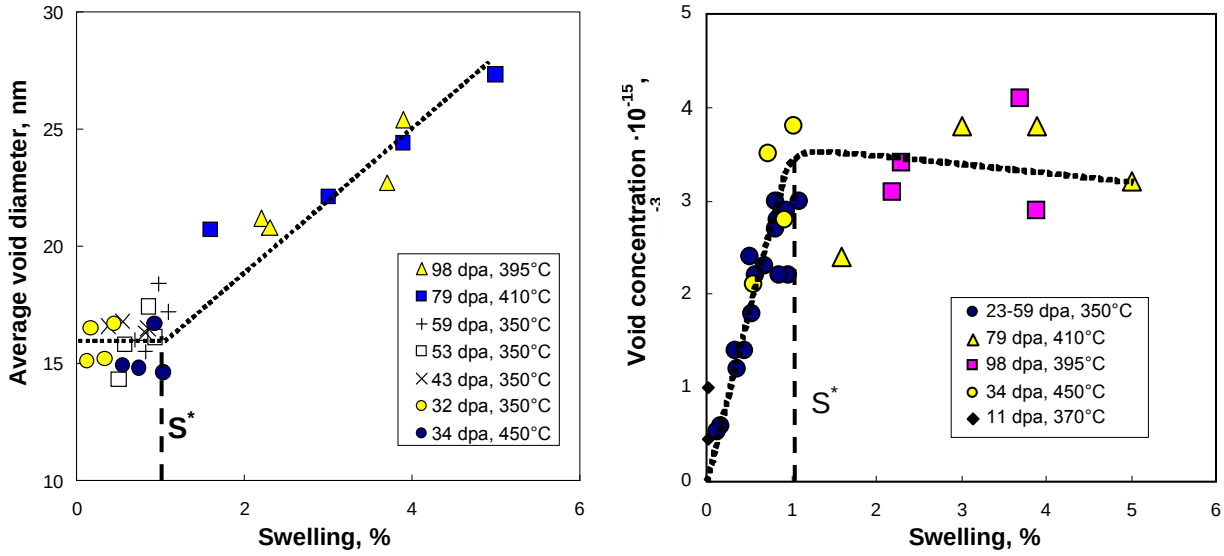


a) b)

Fig. 16. Average void diameter (a) and void concentration (b) versus swelling for 16Cr-15Ni-3Mo-Nb steel irradiated in BOR-60 fast reactor at $T_{irr}$ = 350÷450°C by various neutron doses [36, 38].

Under neutron irradiation together with swelling radiation creep occurs in a material. It is clear that radiation swelling results in increasing stress in a component and radiation creep – in decreasing stress. That's why for calculation of SSF in a component it is necessary to predict not only swelling, but radiation creep too. As a common case the creep rate may be calculated by formula [39]

$$\xi^c_{eq} = (B_0 \frac{dD}{dt} + \omega \cdot \dot{S}_w) \cdot \sigma_{eq}, \qquad (19)$$

where $\xi^c_{eq}$ is equivalent creep rate; $\frac{dD}{dt}$ is dose rate; $B_0$ and $\omega$ are material constants.

In Eq. (19) the parameter $\dot{S}$ or the parameter $\dot{S}_0$ may be taken as $\dot{S}_w$ and there was no sufficient good validation for one or another variant. Analysis of available test results performed by us in [36] has shown that the most adequate prediction may be obtained by Eq. (19) with $\dot{S}_w = \dot{S}$. This conclusion is in particular confirmed by the data in Fig. 17. The test results in Fig. 17 are taken from [37].

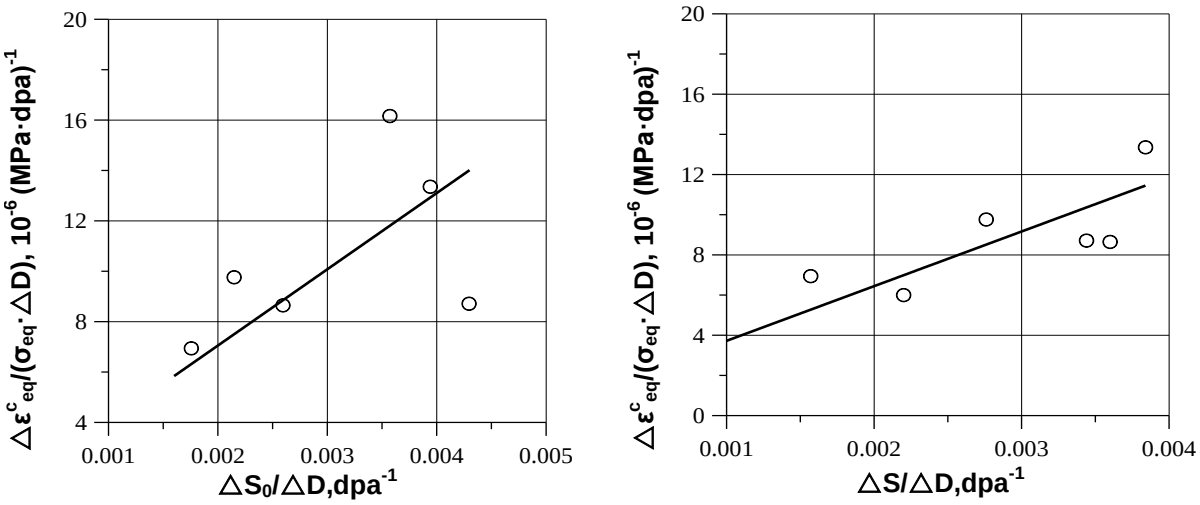


Fig. 17. Comparison of the test results from [37] and the predicted curves calculated by Eq. (19) with $\dot{S}_w = \dot{S}_0$ (a) and $\dot{S}_w = \dot{S}$ (b)[36].

**Embrittlement of 18Cr-10Ni-Ti steel due to swelling.** To investigate the effect of swelling on mechanical properties two sets of specimens were irradiated practically by the same neutron dose, but at different temperatures. For the first set $T_{irr}$ is equal to 320÷340°C, swelling for this case was close to nil. For the second set $T_{irr}$ is equal to 400÷450°C; swelling for this set varies from 3% up to 13%.

The test results on uniaxial tension are represented in Fig. 18. From this figure it is seen that swelling very strongly affects the fracture strain and the type of temperature dependence of fracture strain. If $S > S_{crit}^{\gamma\to\alpha}$ ($S_{crit}^{\gamma\to\alpha}$ is some critical value of swelling) then the dependence $\varepsilon_f(T_{test})$ is typical for BCC metal having ductile-to-brittle transition (DBT). It was found that the root cause of ductile-to-brittle transition in austenitic steels is the phase $Fe_\gamma \to Fe_\alpha$ transformation caused by swelling [31-34]. Swelling is caused by nucleation and growth of voids. Under irradiation Ni segregates on various free surfaces, namely, on void surfaces and grain boundaries. As a result, nickel-rich regions arise near voids and on grain boundaries. These processes result in $Fe_\gamma \to Fe_\alpha$ transformation due to depletion of nickel in austenitic matrix and solid solution destabilization.

As seen from Fig. 18b for $S \geq S_{crit}^{\gamma\to\alpha}$ = 7% the fracture strain is very small at $T < T_{tr}$ ($T_{tr}$ is temperature of DBT) and becomes close to nil at T=20°C.

Radiation swelling results in radiation embrittlement not only due to $Fe_\gamma \to Fe_\alpha$ transformation. According to experimental results in [40, 41] for $S \geq S_{crit}^{r.c.} \approx$ 10-13% sharp embrittlement of austenitic steels is observed even at $T > T_{tr}$, so that tensile specimens rupture at $\sigma < \sigma_{0.2}$. By other words, for S > 10-13% the fracture strain is close to nil and strength parameters also decrease sharply. At the same time fracture on micro-scale happens on the mechanism of vacation void growth and coalescence, i.e. may be described as ductile. Analysis of causes for such sharp embrittlement and its modeling have been performed in [42].

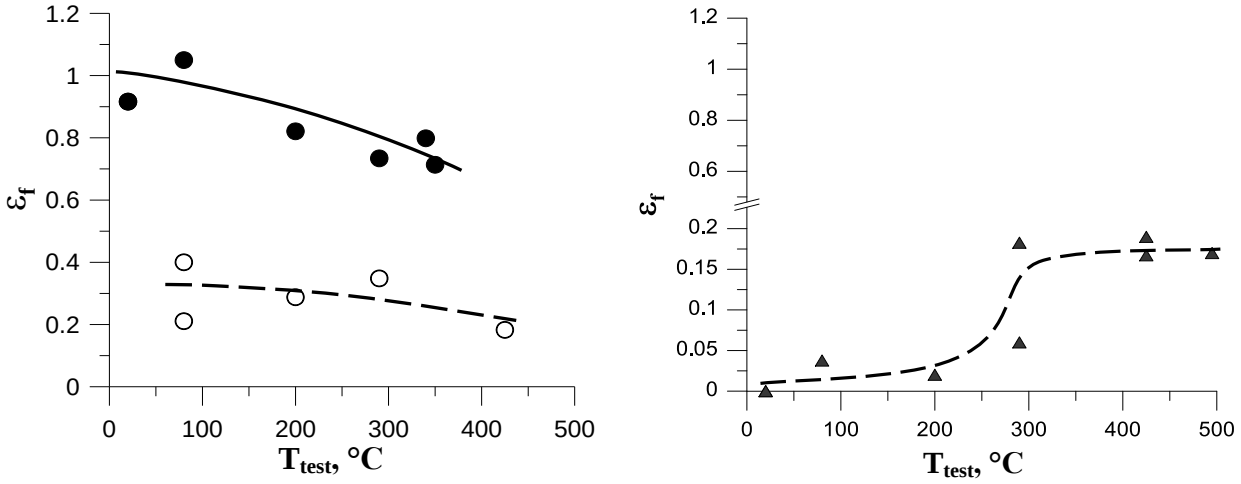


a) b)

Fig. 18. The temperature dependence of fracture strain $\varepsilon_f(T_{test})$ for irradiated 18Cr-10Ni-Ti steel and its weld metal with various values of swelling [31, 33]:
a) – – – - $S < S_{crit}^{\gamma\to\alpha}$ ; ——— - no swelling; b) – – – - $S > S_{crit}^{\gamma\to\alpha}$ ; ($S_{crit}^{\gamma\to\alpha}$ =7%).

It has been found that sharp embrittlement of a material is caused by two processes. The necessary one is inhomogeneous swelling void distribution that is a result of void coalescence at some level of swelling. This process may lead to local material fracture at low stress, i.e. to microcrack initiation under low stress. Unstable growth of this microcrack up to macro-fracture (fracture of specimen) without increase of imposed stress is considered as sufficient condition for sharp embrittlement. This unstable growth occurs due to nano-scale of vacation void sizes and void ligaments when material is loaded on a zone with very small sizes (~80÷400 nm) being more less than grain size.

Thus, from engineering viewpoint optimal structure of internals should be structure for which maximum swelling $S < S_{crit}^{\gamma\to\alpha}$ for the end of lifetime. If service temperature is never less than $T_{tr}$ for all service conditions (including transient ones) or steel with high content of Ni is used for which $Fe_\gamma \to Fe_\alpha$ transformation never happens then it is possible to admit $S < S_{crit}^{r.c.}$.

If for some internals components zones arise with $S \geq S_{crit}^{\gamma\to\alpha}$ or $S \geq S_{crit}^{r.c.}$, these zones should be considered as zones with limit embrittlement in which fracture may occur in any time. By other words, these zones should be schematized as crack-like flaws with sizes equal to limit embrittlement zones sizes, and internals structural integrity should be assessed allowing for these flaws.

It means that for calculation of structural integrity of internals component with cracks (that are zones with limit embrittlement or cracks arising due to corrosion cracking) the fracture toughness for $Fe_\gamma$ material should be known. (Fracture toughness for $Fe_\alpha$ material is not required as such zone is schematized as crack.) Moreover, a criterion of stability of a crack should be formulated for ductile fracture mode. It should be noted that fracture toughness should be predicted with account taken of swelling.

New simple criterion of crack stability for ductile fracture is formulated in [43] as follows. Unstable crack growth does not happen if the following condition is fulfilled

$$J^e < J_c, \tag{20}$$

where $J^e$ is elastic part of J-integral; $J_c$ is critical value of J-integral by crack start criterion.

Criterion (20) has several advantages as compared with universally-accepted criteria. Crack stability is often considered with crack start criterion, i.e. instead of Eq. (20) the condition is used as

$$J < J_c, \tag{21}$$

Eq. (21) is physically validated for brittle fracture of BCC material. For BCC materials condition $J = J_c$ means not only start but also unstable crack growth. For ductile fracture condition $J = J_c$ means only crack start but not growth. Therefore for $Fe_\gamma$ materials that rupture only by ductile mechanisms (here we exclude corrosive intergranular cracks) condition (21) appears to be rather conservative.

Comparison of conditions (20) and (21) has shown the following. For small scale yielding (SSY) $J = J^e$ and conditions (20) and (21) coincide. For large scale yielding (LSY) $J^e < J$, and, hence, condition (20) is less conservative than (21).

To decrease conservatism the condition written as [44]

$$J = J_R(\Delta a), \tag{22}$$

$$\frac{\partial J}{\partial a} < \frac{dJ_R}{da}, \tag{23}$$

where $J_R(\Delta a)$ is so-called $J_R$-curve; a is crack length and $\Delta a$ is a ductile crack extension.

Conditions (22) and (23) are often used instead of (21).

For application of conditions (22) and (23) it is necessary to know $J_R$-curves for irradiated materials and the dependence of J integral on crack size allowing for inner stresses from swelling and temperature gradients. It is clear that these tasks are very complex. That's why application of condition (20) is easier than (22) and (23).

The value of $J^e$ may be calculated from SIF calculated with weight functions. Stresses for SIF calculation are calculated by viscous –elastic -plastic problem solution [43] for component without crack.

The dependence of $J_c$ on neutron dose and test temperature may be calculated according to [45] by equation

$$J_c(T_{test}, D) = C \cdot \sigma_Y(T_{test}, D) \cdot \left[1 - A_\varepsilon \sqrt{1 - \exp(-B_\varepsilon D)}\right], \tag{24}$$

where C=0.25 mm; $A_\varepsilon$ = 0.93; $B_\varepsilon$=0.2 $(dpa)^{-1}$, dpa is displacement per atom.

Yield strength of material without swelling for different doses and test temperatures in common case may be calculated by the following equations [46]

$$\sigma_Y(T_{test}, D) = \sigma_Y^0(T_{test}) + \Delta\sigma_Y(D), \tag{25}$$

$$\sigma_Y^0(T_{test}) = \sigma_{YG} + \beta \cdot \exp\left(-h \cdot (T_{test} + 273)\right), \tag{26}$$

$$\Delta\sigma_Y(D) = A_{\sigma_Y} \cdot \sqrt{1 - \exp(-C_{\sigma_Y} \cdot D)}, \tag{27}$$

where $\sigma_Y^0(T_{test})$ is the temperature dependence of yield strength for material in unirradiated condition, $\Delta\sigma_Y(D)$ is the dependence of yield strength increment on neutron dose, $\sigma_{YG}$, $\beta$, h, $A_{\sigma_Y}$ and $C_{\sigma_Y}$ are material constant.

Eq. (24) has been obtained on the basis of the fracture strain criterion and treatment of large data base of experimental results on fracture toughness. Eq. (24) provides the $J_c$ values with 5% confidence probability, i.e. 95% of all the data lie above the curve. Comparison of the test results and the curve (24) is shown in Fig. 19.

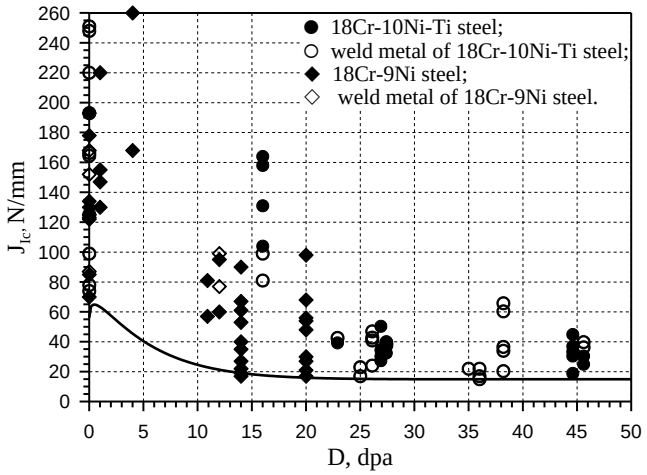


Fig. 19. Fracture toughness for the base and weld metals of austenitic 18Cr-10Ni-Ti and 18Cr-9Ni steels in initial and irradiated conditions at $T_{irr}$=330÷370°C; dots – test results at temperatures from 20 to 300°C [45, 48, 49], the curve – prediction by Eq. (24) for $T_{irr}$=300°C;

The effect of swelling on fracture toughness may be predicted with the physical-and mechanical model of ductile fracture for irradiated austenitic steels developed in [47]. This model allows the adequate prediction of $\varepsilon_f$ and $J_c$ for irradiated austenitic steels both with and without swelling. (The latter is typical for low irradiation temperatures.) As an illustrative example, in Fig. 20 the experimental and predicted values of $\varepsilon_f$ are given for various swelling levels.

On the basis of the ductile fracture model [47] the effect of swelling on fracture toughness has been predicted. The predicted dependence of the ratio $\frac{J_c^S}{J_c^{min}}$ on swelling is shown in Fig. 21. Here $J_c^S$ is fracture toughness for irradiated specimen with swelling and $J_c^{min}$ is $J_c$ value calculated by Eq. (24) for $D \to \infty$, i.e. $J_c^{min}$ is minimum $J_c$ value for material without swelling: $J_c^{min} \approx 14$ N/mm.

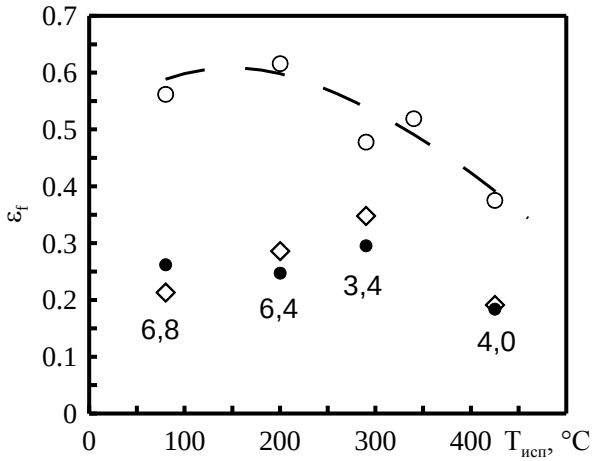


Fig. 20. The temperature dependencies $\varepsilon_f^{exp}$ and $\varepsilon_f^{calc}$ for weld metal of 18Cr-10Ni-Ti steel irradiated up to 46÷49 dpa with and without swelling: open dots – test results for weld metal without (o) and with (◇) swelling (the swelling values in % are given near dots); ● - the $\varepsilon_f^{calc}$ value for weld metal with swelling; — — — - the predicted $\varepsilon_f^{calc}(T)$ curve for weld metal without swelling.

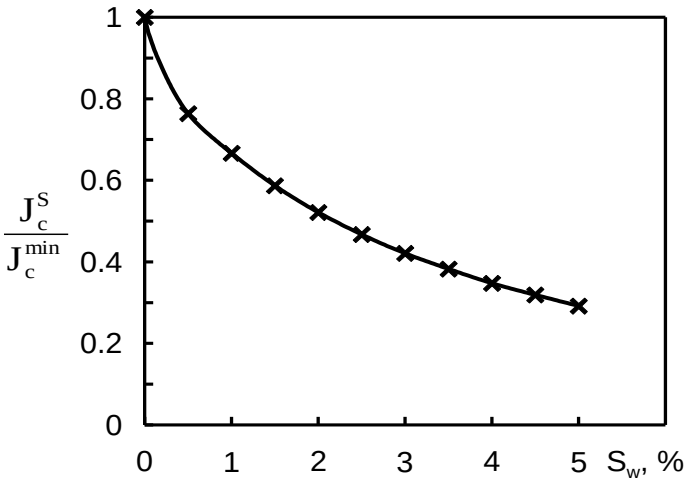

Fig. 21. The predicted effect of swelling on fracture toughness.

As seen from Fig. 21, swelling results in significant decrease of fracture toughness even as compared with low value $J_c^{min}$ although the facture mode is ductile.

**Irradiation Assisted Stress Corrosion Cracking (IASCC) of Austenitic Steels.** As it was mentioned above unirradiated austenitic stainless steel (SS) has high resistance to Stress Corrosion Cracking (SCC) especially in primary circuit deoxygenated water of WWER. At the same time operation experience [50] and laboratory investigations [51-55] have shown the irradiation effect on the susceptibility of SS to intergranular (IG) SCC.

In work [56] the method for assessment of IASCC resistance in WWER water for SSs has been developed. Scheme of the irradiation effect on initiation and growth of crack is shown in Fig.22.

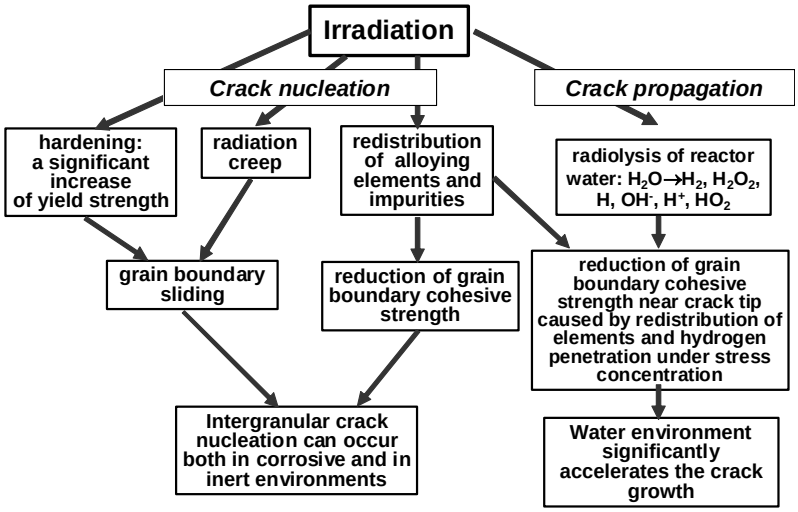

Fig. 22. Scheme of the irradiation effect on initiation and growth of crack.

From the scheme in Fig. 22 one important finding should be emphasized: intergranular crack nucleation can occur both in corrosive and in inert environments. Necessary condition for such mode of fracture is strong hardening of grains for which deformation at $\sigma<\sigma_{0.2}$ occurs mainly at the expense of grain boundary sliding. This conclusion is confirmed by the experimental results in [57] that have revealed intergranular initiation of crack in deoxygenated water for strong cold worked

unirradiated SS. On the basis of the scheme in Fig. 22 the stress-damage dose curve was introduced as shown in Fig. 23 [56, 58]. This curve is the dependence of some threshold stress $\sigma_{th}$ IASCC on neutron dose. For a given neutron dose, if stress is less than $\sigma_{th}^{IASCC}$ SCC does not happen for any exposition time. If stress is large than $\sigma_{th}^{IASCC}$ SCC happens and time to failure is determined by the dependence of equivalent stress on time, depending on neutron dose (Fig. 23b).

We introduced parameter $\Lambda$ equal to the ratio of equivalent stress to threshold stress. The dependence of this ratio on time to failure may be taken as independent function of neutron dose.

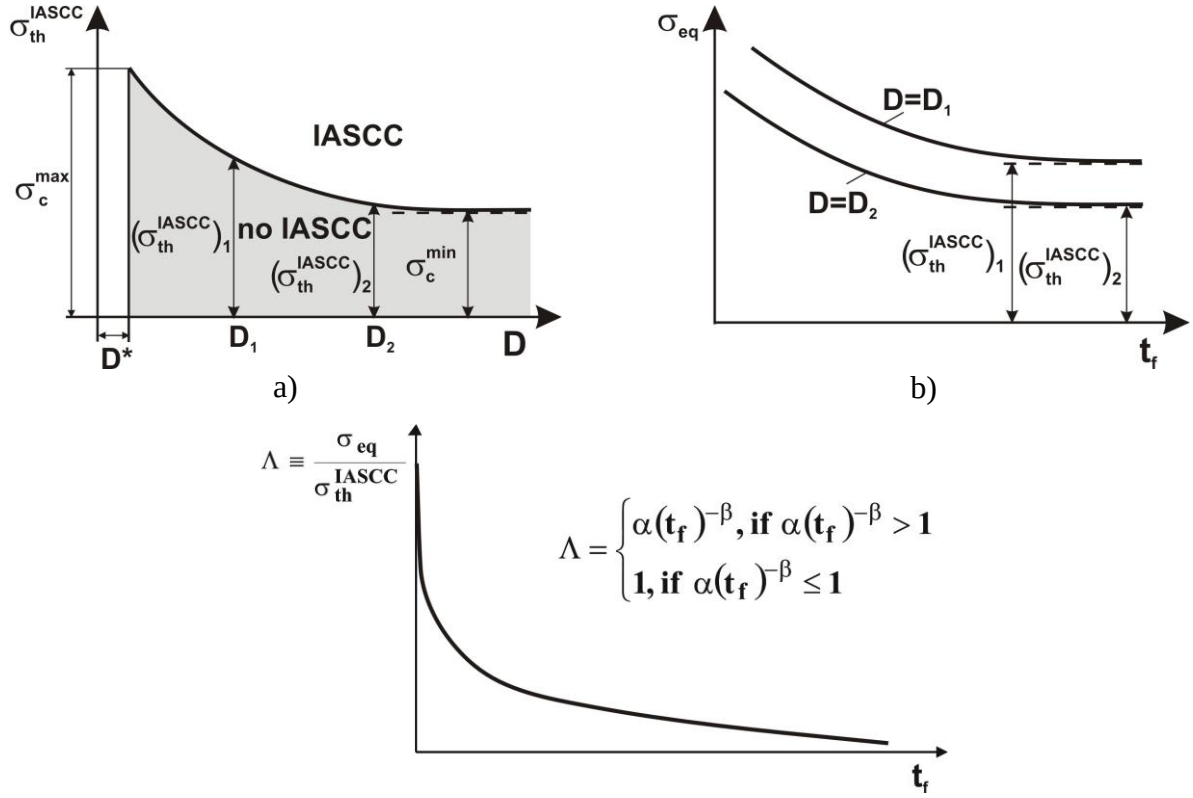


Fig. 23. The stress-damage dose curve (a, b) and the dependence of $\Lambda$ on $t_f$ (c) which is invariant to dose level.

According to IASCC model [56, 58] the dependence $\sigma_{th}^{IASCC}(D)$ is given by the equation

$$\sigma_{th}^{IASCC} = (\sigma_c^{max} - \sigma_c^{min}) \cdot \exp[-b(D-D^*)] + \sigma_c^{min} \quad \text{for } D \ge D^*,$$

where $\sigma_c^{max} = \sigma_{ul|D=D^*}$; $\sigma_c^{min} = \sigma_{Y|D=0}$; $\sigma_{ul}$ – ultimate strength; D* is threshold dose (at D<D* SCC does not happen).

For steels of 304, 316 and 18Cr-10Ni-Ti grades it may be taken

$$\sigma_c^{max} = 632 \text{ MPa}, \ \sigma_c^{min} = 217 \text{ MPa}, \ b = 2.56*10^{-2}, \ D^* = 3 \text{ dpa}.$$

The proposed dependence $\sigma_{th}^{IASCC}(D)$ and available test results are shown in Fig. 24. As it is seen, the proposed curve is in good agreement with available data.

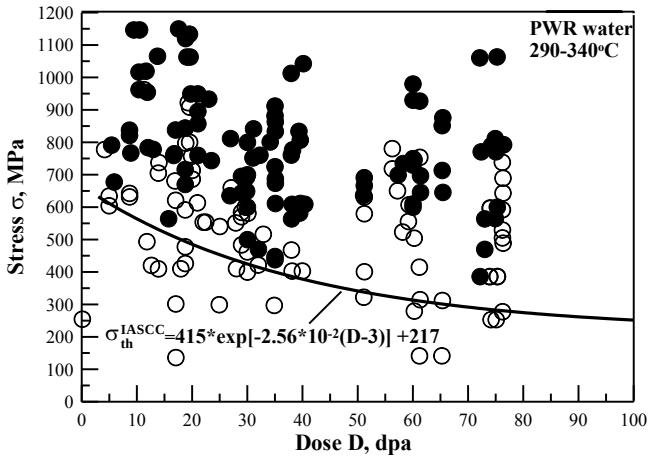


Fig. 24. The dependence $\sigma_{th}^{IASCC}(D)$ and the experimental data on IASCC of SSs [51-55]: ● - failure; ○ - no failure.

**Intermediate conclusion.** Thus the basic mechanisms of degradation for materials of WWER internals and methods for integrity and lifetime assessment for internals components have been presented in this section. In view of the limited volume of article generalization and the analysis of the experimental data on crack growth rate in WWER water environment are not considered, but this material can be found in [50, 56, 59].

## Fast Neutron Reactor

Structural components of fast reactor with sodium coolant of BN type work under high neutron flux and high temperatures when the creep processes occur. Critical event for these components is determined by fracture caused by long-term cyclic and static loading under creep and irradiation.

For assessment of strength and lifetime of structural components of BN reactor the creep-rupture and fatigue properties have to be determined for various neutron flux and time duration of $(3\div5)\cdot10^5$ hours. Two problems arise when obtaining these properties. Firstly, the creep-rupture properties differ for material after and during irradiation, and the properties of post-irradiated materials do not provide conservative estimation. Secondly, direct in-reactor experimental data are restricted to time of $t \le 10^4$ h.

Available extrapolation methods (Larson-Miller, Sherby-Dorn, Manson-Haferd) cannot be used for predicting the creep-rupture properties for long-term service under irradiation. The reason is that these methods convert the lifetime $t_f$ and temperature T into a single parameter, however, the lifetime $t_f$ is affected not only by T and by neutron flux Φ. Moreover, when increasing T the influence of neutron irradiation decreases and, as a result, the same damage cannot be modelled for less time at higher temperature.

If technological defects or stress concentrators are revealed in structural component the lifetime for crack growth stage may be significantly larger than for crack initiation stage and, hence, the lifetime of structural component is mainly determined by crack growth stage. It means that the crack growth rate has to be predicted for austenitic steels under creep and irradiation. Approach recommended in RCC-M Standard for description of the crack growth rate as a function of C*-integral may be used but has to be modified to take into account the properties of material under irradiation.

For assessment of the lifetime of structural components of BN reactor the lifetime has to be also predicted under cyclic loading that is accompanied by creep and neutron irradiation.

For long-term prediction of the above properties for austenitic steels, a physical-and mechanical model of intercrystalline fracture has been developed [60, 61]. The model is based on the plastic

collapse criterion of a unit cell (containing a grain boundary with voids) and includes the equations for nucleation and growth of voids on a grain boundary caused by creep strain and vacancy diffusion allowing for the effect of neutron flux and fluence.

The effect of neutron irradiation on the creep-rupture properties may be illustrated with scheme shown in Fig. 25. It is seen that neutron irradiation accelerates integranular void evolution and decreases the creep-rupture properties by two mechanisms. As neutron dose increases (measured by displacement per atom or neutron fluence) a fraction of intercrystalline sliding in material deformation increases also and, hence, the intercrystalline void nucleation rate increases. Irradiation accelerates diffusion processes in a material that results in increasing the creep rate and void growth rate on vacancy mechanism. As s result, the void nucleation rate on grain boundary accelerates, and hence, the creep-rupture stress and strain decrease.

As followed from Fig. 25, the post-irradiated creep-rupture properties (the neutron flux $\Phi$=0) are higher than properties obtained in-reactor tests when $\Phi \neq 0$ as for $\Phi$=0 the void growth rate and creep rate do not increase as compared with unirradiated material.

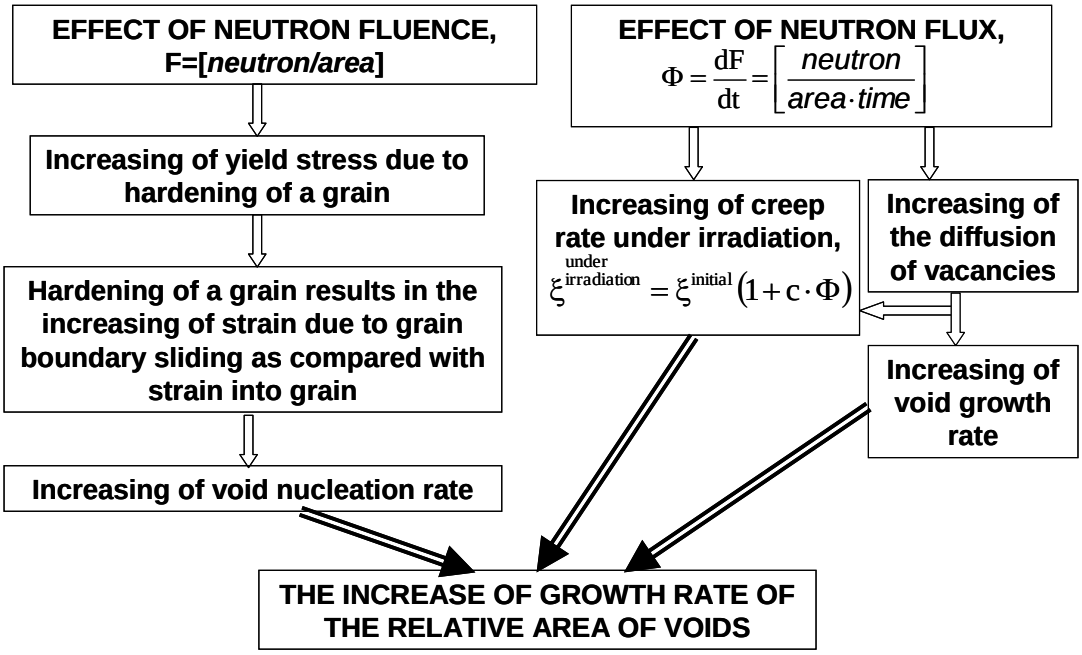


Fig. 25. Acceleration of integranular void evolution under creep due to neutron irradiation (scheme).

The intercrystalline fracture model [60 - 62] has been verified for unirradiated austenitic steels and for steels tested in reactor. Some examples are shown in Fig. 26 and 27. In Fig. 26 the creep-rupture properties are represented for 18Cr-10Ni-Ti steel in initial conditions tested at different temperatures. It should be noted that for calibration of the model parameters the data are only used as obtained for time $t \leq 10^3$ hours at T=600$^o$C. In Fig. 27 the creep-rupture curves are shown for 18Cr-10Ni-Ti steel in unirradiated condition and for in-pile tests. As seen, the predicted curves are in good agreement with the test results.

Thus, these examples show that the developed model allows the adequate prediction of the creep-rupture properties for various temperatures and neutron fluxes.

The developed model allows also the prediction of material properties for various triaxial stress state that provides a possibility to use the model for prediction of the crack growth rate under creep and irradiation. The proposed procedure [64] is the following. Crack growth is schematized as consecutive fracture of unit cell near the crack tip.

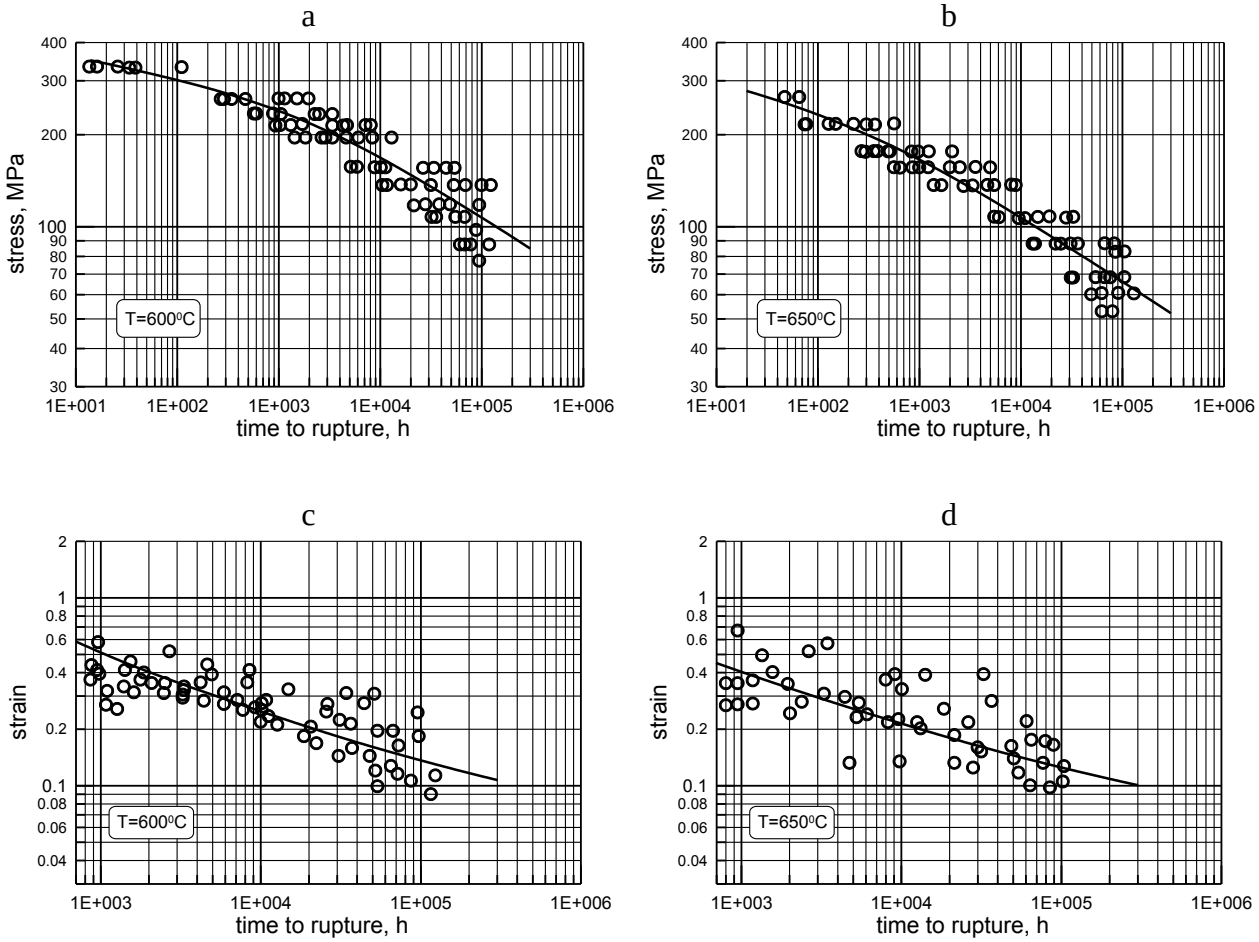


Fig. 26. The creep-rupture strength (a, b) and strain (c, d) for 18Cr-10Ni-Ti steel at T=600°C (a, c) and T=650°C (b, d): (——) – calculation by the model; (○) – experimental data.

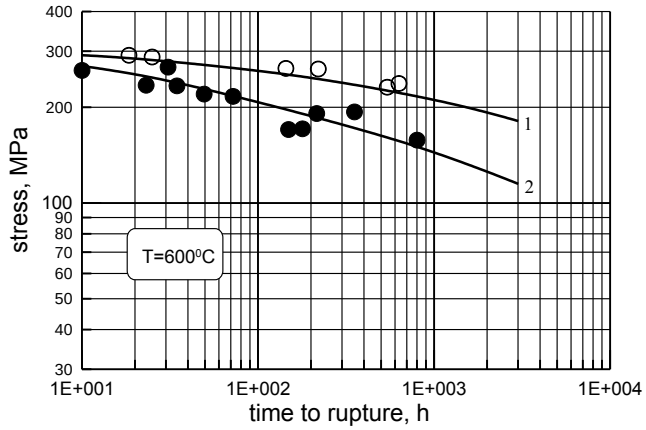


Fig. 27. Comparison of the calculated curves on creep-rupture stress with experimental data at T=600°C for 18Cr-10Ni-Ti steel [63]: curves 1 and 2 – calculation by the model; O, ● - experimental data for material in initial condition and for in-pile tests ($\Phi=1\cdot10^{13}$ n/cm$^2$s (E>0.1 MeV)).

Then the crack growth rate $\frac{da}{d\tau}$ may be calculated by formula

$$\frac{da}{d\tau} = \frac{d\rho}{\tau_f^{uc}}, \tag{28}$$

where $\rho_{uc}$ is unit cell size, $\tau_f^{uc}$ is rupture time for unit cell.

Then the coefficient of acceleration of crack growth rate ω may be calculated by formula

$$\omega \equiv \frac{\left(da/d\tau\right)^{irr}}{\left(da/d\tau\right)^{initial}} = \frac{\left(\tau_f^{uc}\right)^{initial}}{\left(\tau_f^{uc}\right)^{irr}}, \tag{29}$$

where the superscripts "initial" and "irr" are related to material tested in initial condition and tested under irradiation.

The parameter ω is calculated according to the scheme shown in Fig. 28.

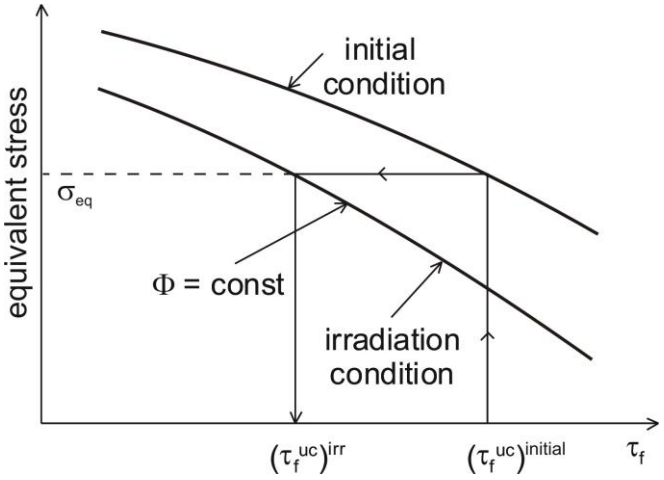


Fig. 28. Scheme for calculation of the crack growth rate under creep and neutron irradiation.

Creep-rupture strength for unit cell near the crack tip is calculated for stress-and-strain fields near the crack tip under creep with the intercrystalline fracture model [60, 61].

For unirradiated material the crack growth rate under creep is calculated according to [65] as

$$\left(\frac{da}{d\tau}\right)^{initial} = A_r\left(C^*\right)^{n_r}, \tag{30}$$

where $A_r$ and $n_r$ are material constants; $C^*$ is so-called $C^*$ - integral.

Then from (29) and (30) we have

$$\left(\frac{da}{d\tau}\right)^{irr} = \omega \cdot A_r\left(C^*\right)^{n_r}. \tag{31}$$

At common case the parameter ω depends on $\left(\frac{da}{d\tau}\right)^{initial}$ and neutron fluence F and flux Φ. Indeed, loading and irradiation of a material near the initial crack tip (shaded area 1 in Fig. 29) occur simultaneously. At the same time irradiation of a material in shaded area 2 occurs all time during crack growth from position 1 to 2 so that when the crack tip reaches position 2, simultaneous loading and irradiation near its tip occur for preliminary irradiated material (see Fig. 29).

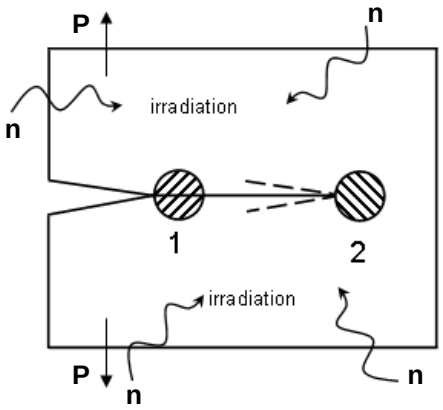


Fig. 29. The effect of neutron flux and neutron fluence on crack growth rate under creep.

Calculations performed by the model shows [64] that the curves describing creep-rupture strength of unit cell for initial condition and under irradiation are practically parallel. Hence, it is possible to assume that ω doe not depend on $\left(\frac{da}{d\tau}\right)^{initial}$. In [64] it has been shown that the parameter ω may be written as

$$\omega = \omega_1(\Phi) \cdot \omega_2(F) \tag{32}$$

The dependencies $\omega_1(\Phi)$ and $\omega_2(F)$ calculated with the model [60, 64] are shown in Fig. 30.

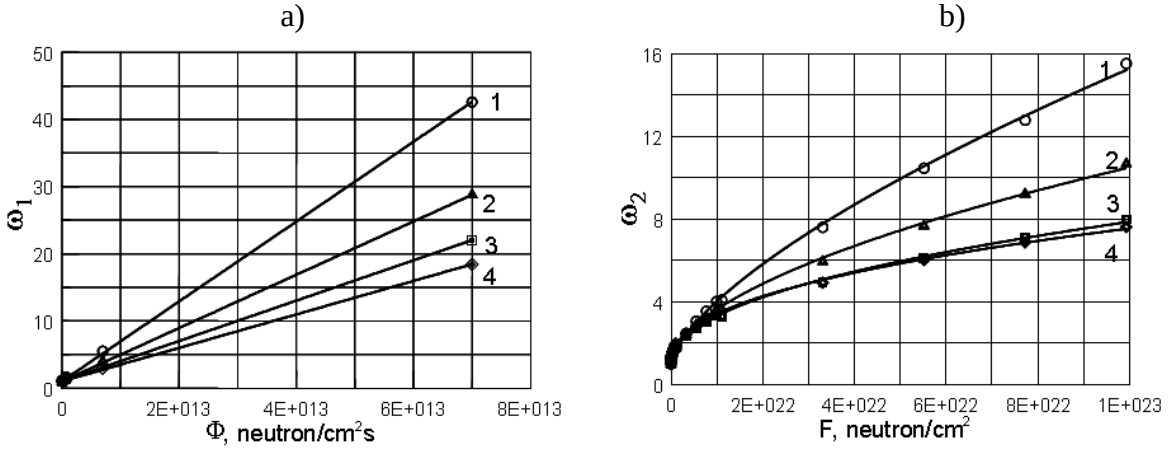


Δ, O, □, ◇ - calculated points; —— – approximation by formula, 1 – 550⁰C; 2 – 600⁰C; 3 – 650⁰C; 4 – 700⁰C.

Fig. 30. The dependences of the parameter $\omega_1$ on neutron flux (a) and of the parameter $\omega_2$ on neutron fluence (b) at various temperatures.

The above procedure for prediction of the creep-rupture properties and the crack growth rate under creep may be used for static loading. Now the procedure will be considered for cyclic loading. This procedure is based on the following considerations.

1) The Coffin-Manson equation is used in the form [66]

$$\Delta\varepsilon = \varepsilon_f (4N_f)^{-m} + \frac{2\sigma_{cr}}{E(4N_f)^{m_e}}, \qquad (33)$$

where $\sigma_{cr}$ is true fracture stress under creep; $\varepsilon_f$ is fracture strain under creep, $N_f$ is the number of cycles to failure; m and $m_e$ are material constant.

2) The parameters $\sigma_{cr}$ and $\varepsilon_f$ depend on the strain rate $\xi$ in loading cycle as well as on F, Φ and T [67]. The dependencies $\sigma_{cr}(\xi)$ and $\varepsilon_f(\xi)$ for given values of F, Φ and T may be determined from the creep–rupture properties according to the scheme shown in Fig. 31.

3) The creep-rupture properties for different values of F, Φ and T may be calculated by the model [60, 61].

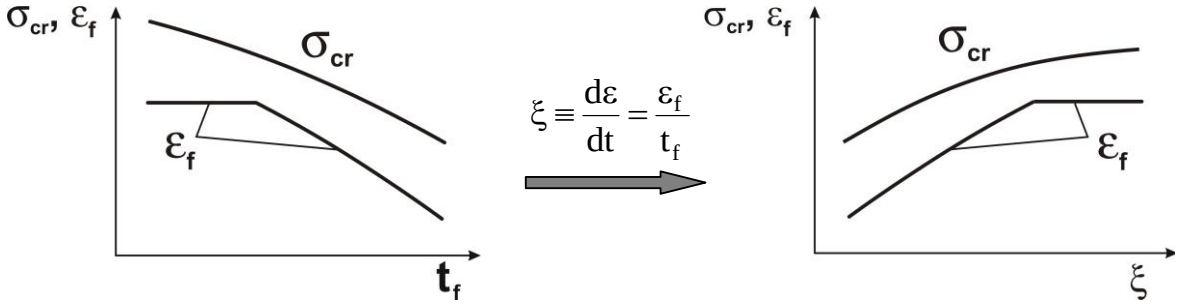


Fig. 31. Scheme for determination of $\sigma_{cr}(\xi)$ and $\varepsilon_f(\xi)$ on the basis of creep-rupture properties.

Comparison of the calculated curves with test results is shown in Fig. 32 for 18Cr-9Ni steel [67, 68]. As seen, the proposed procedure allows the adequate assessment the lifetime $N_f$ for loading with various holds that result in various strain rates in cycle.

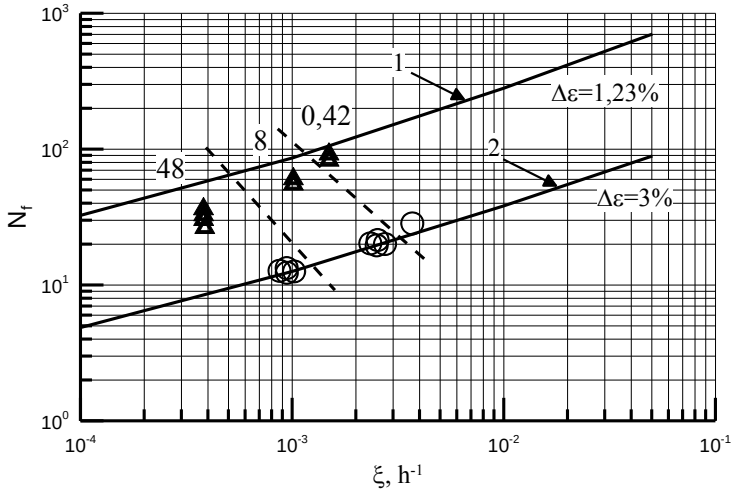


Fig. 32. Comparison of the test results with the calculated curves for thermal-cyclic loading with hold at maximum temperature in cycle: curves 1 and 2 – calculation for the strain ranges Δε=1.23 % and ε=3 % respectively; Δ, O – tests for strain range Δε=3 % and Δε=1.23 % respectively and different hold times in hours as shown near the dots; the dashed line separates the test results for different hold times [68].

**Intermediate Conclusion.** The calculated results with the intercrystalline fracture model, the methods proposed for prediction of mechanical properties and the formulated criteria of limit states for BN reactor components are a basis for new Russian Standard for calculation of strength and lifetime for BN reactor components.

## Conclusion

On the basis at presented approaches, models, methods and experimental investigations the following Russian standards in field structural integrity of NPP equipment with regard for prediction of change material properties during operation were created.

RD EO 0606-2005. "Calculation Method for Evaluation of Brittle Strength of WWER RPV During Operation. MRKR-SKhR-2004"

RD 1.6.1.08.0018-2007 "Method for Strength Calculation for WWER-1000 Internals for Service Life Extension"

RD EO 1.1.2.09.0789-2009 Method for determination of fracture toughness on the basis of test results of surveillance specimens for strength and lifetime calculation for WWER-1000 RPV

RD EO 1.1.2.09.0714-2011. "Method for Structural Integrity Assessment of Fast Neutron Reactor Components with Sodium Coolant"

## References


[1] K. Wallin: Eng. Fract. Mech. Vol. 19**(**1984), p. 1085-1093.

[2] K. Wallin: Eng. Fract. Mech. Vol. 22**(**1985), p. 149-163.

[3] K. Wallin, in: *Fracture of engineering materials & structures*, edited by Teoh S. and Lee K., Elsevier Applied Science, (1991).

[4] F.M. Beremin: Met.Trans., Vol. 14A (1983), p. 2277-87.

[5] VOCALIST Handbook, in: Proceedings of International Seminar. *Transferability of Fracture Toughness Data for Integrity of Ferritic Steel Component*, November 17-18, 2004, Petten, the Netherlands. EUR 21491 EN. Luxemburg, Office for official Publications of the European Communities (2004)

[6] B.Z. Margolin, V.A. Shvetsova, A.G. Gulenko: Int. J. Pres. Ves. & Piping Vol. 76 (1999), p. 715 - 729

[7] W.A. Weibull: R. Swed. Inst. Eng. Res., Vol. 151 (1939), p. 5-45.

[8] ASTM E 1921-02. Standard Test Method for Determination of Reference Temperature, $T_0$, for Ferritic Steels in the Transition Range, in: Annual Book of ASTM Standards, Philadelphia Vol. 03.01 (2002), p. 1068 - 1084.

[9] J.G. Merkle, K. Wallin, D.E. McCabe: *Technical basis for an ASTM standard on determining the reference temperature, $T_0$ for ferritic steels in the transition range*. (NUREG/CR-5504, ORNL/TM-13631 1999).

[10] B.Z. Margolin, V.A. Shvetsova: Strength of materials Vol. 2 (1992), p. 3-16

[11] B.Z. Margolin, V.A. Shvetsova, G.P. Karzov: Int. J. Pres. Ves. & Piping Vol. 72 (1997), p. 73-87.

[12] B.Z. Margolin, G.P. Karzov, V.A. Shvetsova: Int. J. Pres. Ves. & Piping Vol. 72 (1997), p. 89-96.

[13] B.Z. Margolin, A.G. Gulenko, V.A. Shvetsova: Int. J. Pres. Ves. & Piping Vol. 75 (1998), p. 307-320.

[14] B.Z. Margolin, A.G. Gulenko, V.A. Shvetsova: Int. J. Pres. Ves. & Piping Vol. 75 (1998), p. 843-855.

[15] B.Z. Margolin, A.G. Gulenko, V.A. Nikolaev, L.N. Ryadkov: Int. J. Pres. Ves. & Piping Vol. 80 (2003), p. 817-829.

[16] N.P. O'Dowd, C. F. Shih: J. Mech. Phys. Solids Vol. 39 (1991), p. 989-1015.
[17] N.P. O'Dowd, C. F. Shih: J. Mech. Phys. Solids Vol. 40 (1992), p. 939-963.
[18] B.Z. Margolin, V.A. Shvetsova, A.G. Gulenko, and V.I. Kostylev: Int. J.Pres. Ves. & Piping Vol. 84/5 (2007), p. 320-336.
[19] P. Gilles, in: Proceedings of International Seminar. *Transferability of Fracture Toughness Data for Integrity of Ferritic Steel Component*, November 17-18, 2004, Petten, the Netherlands. EUR 21491 EN. Luxemburg, Office for official Publications of the European Communities (2004), p.312-324.
[20] B.Z. Margolin, E.Yu. Rivkin, G.P. Karzov, V.I. Kostylev, A.G. Gulenko, in: *Proceedings VI Int. Conf.: Material Issues in Design, Manufacturing and Operation of Nuclear Power Plants Equipment.* St-Petersburg, Russia, vol.2 (2000), p. 100-119.
[21] B.Z. Margolin, E.Yu. Rivkin, G.P. Karzov, V.I. Kostylev, A.G. Gulenko, in: *Transaction of the 17th Int. Conf. on Structural Mechanics in Reactor Technology (SMIRT 17),* G01-4, Prague, Czech Republic (2003).
[22] G.P. Karzov, B.Z. Margolin, E.Yu. Rivkin: Int. J. Pres.Ves.Piping Vol. 81 (2004), p. 651-656.
[23] Taylor N.G., Nilsson K.-F., Minnebo P., et al.: *An investigation of the transferability of Master Curve technology to shallow flaws in reactor pressure vessel applications*. NESC-IV Project. Final report EUR 21846 EN. European Commission DG-JRC/IE, Petten, The Netherlands, (2005).
[24] W. J. McAfee, B. R. Bass, W. E. Pennell and J. W. Bryson, in: *USNRC Report NUREG/CR-4219 (ORNL/TM-9593/V12&N1)* (1996), p. 16-24.
[25] B.Z. Margolin and V.I. Kostylev: Int. J. Pres. Ves. & Piping Vol. 75 (1998), p.589-601.
[26] Guidelines on pressured thermal shock analysis for WWER nuclear power plants. IAEA, 2006.
[27] Unified procedure for lifetime assessment of components and piping in WWER NPPs "VERLIFE". Report number: COVERS-WP4-D4.10. EC (2008).
[28] B.Z. Margolin, V.I. Kostylev, E. Keim: Int. J. Pres. Ves. Piping Vol. 81 (2004), p. 949-959.
[29] Dana Lauerova, Vladislav Pistora, Milan Brumovsky, Milos Kytka, in: *Proceedings of PVP2009 ASME Pressure Vessels and Piping Division Conference*, July 26-30, Prague, Czech Republic, PVP2009-77287 (2009).
[30] Task 4. Analysis of structural integrity of VVER internals, in: *Proc. of Seminar for the Dissemination of the Results of the Project TACIS R2.01/02*, OKB "GIDROPRESS", Podolsk, Russia, 25 Feb. (2010).
[31] B. Z. Margolin, I. P. Kursevich, A. A. Sorokin, A. N. Lapin and V. I. Kokhonov, et al.: Strength of Materials Vol. 41(6) (2009), p. 593-602.
[32] B. Z. Margolin, I. P. Kursevich, A. A. Sorokin, N. K. Vasina and V. S. Neustroev: Strength of materials Vol. 42(2) (2010), p. 144-153.
[33] D.L Porter et al., in: *19th International Symposium, ASTM STP 1336*, (2000), p.884-893.
[34] B. Margolin, A. Sorokin, I. Kursevich, V. Neustroev, in: *Proc. of 7th International Symposium "Contribution of materials investigations to improve the safety and performance of LWRs"*, France, Avignon, 26-30 September (2010).
[35] N.K. Vasina, B.Z. Margolin, A.G. Gulenko, I.P. Kursevich: Voprosy materialovedeniya (Problems of materials science) Vol. 4(48) (2006), p. 69-89 (in Russian)
[36] B.Z. Margolin, A.I. Murashova, V.S. Neustroev: Voprosy materialovedeniya (Problems of materials science) Vol. 68(4) (2011), p. 124-139 (in Russian)
[37] M.M. Hall, J. E. Flinn: J. Nucl. Mat. Vol. 396 (2010), p. 119–129
[38] V. S. Neustroev, Z. E. Ostrovsky, V. K. Shamardin: J. Nucl. Mat. Vol. 329-333 (2004), p. 119–129.
[39] K. Erlich: J. Nucl. Mater. Vol. 100 (1981), p. 149–166.

[40] V.S. Neustroev, F.A. Garner: Fusion Materials Vol. 43. Semiannual Progress Report for Period Ending December 31 (2007), p. 109–122.
[41] A.V. Kozlov, I.A. Portnyh, S.V. Bryushkova, E.A. Kinev: FMM (Physics of metal and metals science) Vol. 95(4) (2003), p. 87-97 (in Russian)
[42] B.Z. Margolin, A.A. Sorokin: Voprosy materialovedeniya (Problems of materials science) Vol. 69(1) (2012), p. 148-162 (in Russian)
[43] B.Z. Margolin, V. N. Fomenko and A. A. Sorokin: Strength of Materials Vol. 42(3) (2010), p. 258-271.
[44] K. Hellan: *Introduction to Fracture Mechanics* (McGraw- Hill Book Company Inc. 1984).
[45] B.Z. Margolin, A.I. Minkin, V.I. Smirnov et al.: Voprosy materialovedeniya (Problems of materials science) Vol. 53(1) (2008), p.123-138 (in Russian).
[46] A. A. Sorokin, B.Z. Margolin, Kursevich I.P., A.I. Minkin, V.S. Neustroev, S.V. Belozerov: Voprosy materialovedeniya (Problems of materials science) Vol. 66(2) (2011), p. 131-152.
[47] B.Z. Margolin, A. A. Sorokin: Voprosy materialovedeniya (Problems of materials science) Vol. 69(1) (2012), p.126-147 (in Russian)
[48] G.P. Karzov, I.P. Kursevich, A.N. Lapin et al., in: *Radiation Material Science and Structural Integrity of Reactor Materials. Anniversary*, edited by CRISM "Prometey" (2002), p.270. (in Russian)
[49] V.I. Smirnov, B.Z. Margolin, A.N. Lapin, V.I. Kokhonov, A.A. Sorokin: A.A. – Voprosy materialovedeniya (Problems of materials science) Vol. 65(1) (2011), p. 167-183
[50] O.K. Chopra: *Degradation of LWR Core Internal Materials due to Neutron Irradiation* (NUREG/CR-7027, 2010)
[51] J. Conermann, R. Shogan, K. Fujimoto, T. Yonezawa, Y. Tamaguchi, in: *Proc. of 12$^{th}$ Int. Conf. on Environmental Degradation of Materials in Nuclear Power Systems-Water Reactors*, USA, August 14-18 (2005), p. 277-287
[52] P. Freyer, T. Mager, M. Burke, in: *Proc. of 13$^{th}$ Intern. Conf. on Environmental Degradation of Materials in Nuclear Power Systems-Water Reactors*, Canada, August 19-23 (2007)
[53] A. Toivonen, P. Aaltonen, W. Karlsen, U. Ehrnsten, J.-P. Massoud, J.-M. Boursier, in: *Proc. of 6$^{th}$ Intern. Symp. on Contribution of Materials Investigation to Improve the Safety and Peformance of LWRs*, France, Fontevraud, 18-20 September (2006), p. 567-579.
[54] K. Takakura, K. Nakata, N. Kubo, K. Fujimoto, K. Sakima, in: *Proc. of the ASME Pressure Vessels and Piping Division Conference PVR 2009*, Prague, Czech Rebulic (2009), PVP2009-77279
[55] H. Nishioka, K. Fukuya, K. Fujii, T. Torimaru: Journal of Nuclear Science and Technology Vol. 45(10) (2008), p. 1072-1077
[56] V.A. Fedorova, B.Z. Margolin, in: *Proc.of the ASME Pressure Vessels and Piping Division Conference PVR 2009*, Prague, Czech Rebulic (2009), PVP2009-77095.
[57] K. Arioka, T. Yamada, T. Terachi, R.W. Staehle: Corrosion Vol. 62(1) (2006), p. 74-83
[58] B.Z. Margolin, V.A. Fedorova, V.M. Filatov: Voprosy materialovedeniya (Problems of materials science) Vol. 63(3) (2010), p. 105-118 (in Russian)
[59] A. Hojna, M. Ernestova, O. Hietanen, R. Korhonen, L. Hulinova, F. Oszvald, in: *12th Intern. Symp. on Environmental Degradation of Materials in Nuclear Power Systems – Water Reactors*, Colorado, USA, August 7-11 (2011)
[60] B.Z. Margolin, A.G. Gulenko, I.P. Kursevich, A.A. Buchatsky: Strength of materials Vol. 3 (2006), p. 5-22
[61] B.Z. Margolin, A.G. Gulenko, A.A. Buchatsky, in: *Proceedings of ASME 2009 Pressure Vessels and Piping Division Conference PVP2009 July 26-30, 2009*, Prague, Czech Republic (2009), PVP2009-77084

[62] B.Z. Margolin, A.G. Gulenko, I.P. Kursevich, A.A. Buchatsky: Strength of materials Vol. 5 (2006), p. 5-16
[63] S.N. Votinov, V.I. Prohorov, Z.E. Ostrovski: *Irradiated stainless steels* (Nauka, Moscow 1987) (in Russian)
[64] B.Z. Margolin, A.G. Gulenko, A.A. Buchatsky, S.M. Balakin: Strength of materials Vol. 6 (2006), p. 5-16
[65] RCC-MR: Design and construction rules for mechanical components of FBR Nuclear Islands, Appendix A16, Edition 2002, AFCEN, France (2002)
[66] PNAE G-7-002-86. *Standard for strength calculation for equipments and piping of atomic power plants* (Energoatomizdat, Moscow 1989) (in Russian)
[67] B.Z. Margolin, A.G. Gulenko, A.A. Buchatsky and et.al.: Strength of materials Vol. 6 (2008), p. 5-24
[68] V.M. Filatov, Yu. A. Anihomovskiy, D.V. Soloviev, A.N. Vasyutin: Zavodskaya laboratoria (Factory laboratory), Vol.41(4) (1975), p.472-475 (in Russian)